Immediate epileptogenesis: Impact on brain in C57BL/6J mouse kainate model

Sreekanth Puttachary[1], Shaunik Sharma[1], Achala Thippeswamy[1], Thimmasettappa Thippeswamy[1]

[1]Department of Biomedical Sciences, College of Veterinary Medicine, Iowa State University, Ames IA 50011-1250, USA

TABLE OF CONTENTS

1. ABSTRACT

We have recently demonstrated immediate epileptogenesis in the C57BL/6J mouse, the strain that is resistant to kainate-induced neurotoxicity. By using a repeated low dose of kainate, we produced mild and severe *status epilepticus* (SE) models. In the present study, we demonstrate the impact of mild and severe SE, and spontaneous convulsive/nonconvulsive seizures (CS/NCS) on structure and function of the hippocampus, entorhinal cortex, and amygdala at 7, 14 and 28 day post-SE. Immunohistochemistry (IHC) of brain sections confirmed reactive astrogliosis and microgliosis, neurodegeneration, and increased neurogenesis in both groups. The epileptiform spike rate was higher in the severe group during first 12 days, but they decreased thereafter. Morris water maze test confirmed cognitive deficit in both mild and severe groups at 12d post-SE. However, MRI and IHC at 18 weeks did not reveal any changes in the hippocampus. These findings suggest that in C57BL/6J mice, immediate spontaneous CS could be responsible for early brain pathology or vice versa, however, the persistent spontaneous NCS for a long-term had no impact on the brain structure in both groups.

2. INTRODUCTION

The C57BL/6J mouse is genetically resistant to kainate-induced acute neurotoxicity (1-4), which limited the opportunity for researchers to use this strain of mouse as a model of chronic epilepsy. The C57BL/6J mouse also serves as a background strain in the production of certain transgenic mice used in epilepsy research. Therefore, C57BL/6 wild-type mice would be the most appropriate critical control for such studies. The C57BL/6J strain, as an acute model of *status epilepticus*

(SE), also had several disadvantages such as high mortality rate and a huge variability in seizure response to chemoconvulsants, especially for kainate (4-7). We have recently addressed these important issues in the C57BL/6J mice by administering repeated low dose of kainate (5 mg/kg, i.p. at 30 minutes intervals) until they reached stage-3 or -5 seizures (8, 9). This method yielded consistently mild (stage-3) or severe (stage-5) SE in greater than 92 percent of the mice and the SE could last for about 2 hours with less than 7 percent mortality rate (9). Importantly, irrespective of mild or severe SE, this method of inducing SE with kainate also caused immediate epileptogenesis in the C57BL/6J mice (8).

The conventional histological methods such as cresyl violet, hematoxylin and eosin, and fluoro-jade B (FJB) staining of brain sections at early time points (less than or equal to 7 day post-SE), induced by kainate, in the C57BL/6J mouse models produced mixed results with respect to neurodegeneration in the epileptic foci of the brain (2-4, 6, 7). Perhaps, these observations led to a belief that these mice are unlikely to develop epilepsy due to lack of a significant number of neuronal cell loss in the epileptic foci of the brain, unlike in the rat kainate models (10-13). In addition to hippocampal neurodegeneration, subtle changes in the neuronal population in the hilus and the subgranular zone of the dentate gyrus, reactive gliosis in the hippocampus and in other epileptic foci, and neurogenesis and aberrant migration of neuroblasts, could all contribute to epileptogenesis (14-20). The other reason for the dearth of reports on immediate epileptogenesis in C57BL/6J mice is inadequate seizure monitoring (21-25). Using continuous (24/7) remote video-EEG telemetry system, we have recently demonstrated that repeated low dose of kainate injection method induces consistent mild or severe SE (9), and immediate epileptogenesis in the C57BL/6J (8). The unique feature of this model is that the maximum numbers (27 plus or minus 4) of spontaneous convulsive seizures (CS) were observed during the first 4-6 weeks of the SE, in the severe SE group, and they decreased thereafter to less than 5 seizures/month for up to 18 weeks (the maximum recording period) (8). The mild SE also induced immediate epileptogenesis but the numbers of spontaneous CS were less than 5 episodes during the first 4 weeks of the SE and 1 or 2 seizure/month was observed during the remaining recording period. Interestingly, the numbers of spontaneous electrographic NCS were about 20 per day/night cycle in both the severe and the mild SE groups throughout the 18 weeks period (8). Based on these observations, our hypotheses were that i) the severity of the SE will induce hyperexcitability of neurons (increased spike rate), reactive gliosis and neurodegeneration in the epileptic foci of the brain, and will also increase neurogenesis in the dentate gyrus to cause spontaneous CS and NCS during the first 4 weeks ii) these changes in the hippocampus will lead

to cognitive dysfunction during this period, and iii) these changes will begin to decrease by 4 weeks to promote recovery from spontaneous CS. In this study, we tested these hypotheses to understand some of the plausible neurobiological reasons for spontaneous CS and recovery. We compared the elements of epileptogenesis such as EEG correlates, reactive astrogliosis and microgliosis (using glial fibrillary acidic protein (GFAP) and ionized calcium binding adaptor molecule 1 (IBA1), neurodegeneration (FJB + neuronal nuclear antibody, NeuN) and doublecortin (DCX) immunostaining (to label neuroblasts, an indicator of neurogenesis) at 7, 14 and 28 days post-SE. In addition, the impact of immediate epileptogenesis on their cognitive function was assessed using the Morris water maze test. At 18 weeks, the mice were subjected to MRI prior to euthanasia and the brains were processed for histology. The findings from these studies are presented and discussed.

3. MATERIALS AND METHODS

3.1. Animal source and ethics statement

The C57BL/6J male mice, 7-8 weeks old, were purchased from the Jackson Laboratory, ME, USA and maintained under controlled environmental conditions (19°C – 23°C, 12h light: 12h dark), with *ad libitum* access to food and water in the Laboratory of Animal Resources at ISU. All experiments were carried out in accordance with the Institutional Animal Care and Use Committee, ISU, USA (protocol no. 10-12-7446-MR). The surgery was performed under isoflurane anesthesia and aseptic conditions. Appropriate postoperative care was undertaken to minimize pain and discomfort to animals.

3.2. Chemicals and reagents

Kainate (Abcam, USA) was prepared fresh in sterile distilled water at a concentration of 2mg/ml. For perfuse fixation we used: phosphate buffered saline (PBS, all chemicals from Sigma, USA), sodium sulfide perfusate solution in deionized water (48.3 mM sodium sulfide nonhydrate, Sigma, USA; 87mM sodium phosphate monobasic monohydrate, Fisher Chemicals, USA), and 4 percent paraformaldehyde (PFA, Acros Organics, NJ, USA). The primary antibodies and concentration used were as follows: NeuN (1:400, rabbit, EMD Millipore, USA); IBA1 (1:500, goat, Abcam, USA); GFAP (1:400, mouse, Sigma, USA); DCX (1:500, goat, Santa Cruz, USA). Appropriate secondary antibodies tagged with fluorescent dyes (CY3 1:300 or FITC, 1:100) or biotinylated antibodies (1:500) or 4', 6-diamidino-2-phenylindole (DAPI at 0.0001 percent) (all from Jackson ImmunoResearch Laboratories, USA) were used. The chemicals used for preparing the diluting solution in PBS for antibodies (0.1 percent Triton X-100, 2.5 percent donkey serum and 0.25 percent sodium azide) were purchased from Sigma, USA. The fluorochrome conjugates of streptavidin were diluted in PBS alone.

3.3. Mild and severe SE induction with kainate and the experimental groups

We used 70 male mice in this study. Six mice received no drug and they served as control for all time points for immunohistochemistry (IHC) and another 16 mice were used as control for Morris water maze. Further 8 mice were implanted with radiotelemetric device for continuous (24/7) video-EEG recording for 18 weeks, and for MRI, after the induction of SE with kainate. Four mice were used for sham surgery for MRI study. The remaining 36 mice, including the mice that were implanted with the radiotransmitter, were administered a low dose of kainate (5mg/kg, i.p.) which was repeated at 30 minutes intervals to induce mild or severe SE as described previously (8, 9). The seizures during the SE were classified as nonconvulsive seizures (NCS; Racine scale/stage-1 and -2) or CS (Racine scale/stage 3-5). The behavioral seizure quantification during the SE, video-EEG recording procedures, and EEG analyses to detect spontaneous behavioral CS and electrographic NCS have been described in our recent publication (8).

All the mice that received kainate, irrespective of the dose, had continuous stage 1 or 2 seizures (NCS) for greater than 40 minutes. Since C57BL/6J mice response to KA is highly variable, we titrated each mouse with repeated low doses for the development of mild or severe seizures (9). Our previous studies from the C57BL/6J mice have shown that there was no correlation between the doses of KA and the severity of the SE or epileptogenesis or frequency of spontaneous recurrent CS (8, 9). To classify them as mild or severe SE group, we considered total duration of the CS stages during the 2h established SE (8, 9). All those mice that experienced stage-3 seizures (rearing and forelimb clonus) for less than 10 minutes were considered as the mild SE group. These mice never reached stage 4 or 5 seizure. The severe SE group had several episodes of stage 3-5 seizures (rearing and continuous forelimb clonus, repeated rearing and falling, tonic clonic seizures including wild running and jumping) for greater than 10 minutes (8). The behavior of all animals during the period of SE was video recorded and further verified to score offline for the severity of the SE by two more personnel who were unaware of the experimental groups. The telemetry mice were video-EEG recorded continuously for up to 18 weeks to identify the spontaneous CS and electrographic NCS as described previously (8). These experiments were done in parallel with the mild and severe SE group mice that were not implanted with the radiotransmitter. The telemetry mice and four surgery control (sham) mice were euthanized at 18 week, after acquiring MRI images, by perfusion fixation with sodium sulfide and paraformaldehyde under terminal anesthesia with an overdose of pentobarbital sodium (100 mg/kg, i.p.). The remaining mice were euthanized similarly at 7, 14 and 28 days post-SE. During the course of the experiments, the mice were subjected to Morris water maze to investigate the impact of seizures on their cognitive function.

### 3.3.1. Cortical EEG acquisition with continuous video EEG monitoring and analysis

The mice were implanted with a telemetric radiotransmitter (Physiotel and Multiplus ETA-F20, Data Science International (DSI), MN, USA), subcutaneously, 8–10 days before the induction of SE with KA. The electrodes were placed bilaterally on the cortical dura mater through the burr holes (2.5 mm caudal to Bregma and 2 mm lateral to the midline) as described previously (8, 9). The EEG acquisition (Dataquest ART) and analysis were carried out using NeuroScore (DSI) software. The post-SE EEG signals were normalized with the baseline EEG from the same mouse. The epileptiform spikes, the normal baseline spikes, and the spikes due to electrical or mechanical artifacts were distinguished based on individual spike characteristics such as amplitude, duration, frequency, and inter-spike intervals (9). We have previously described different types of epileptiform spikes and CS in this model (8). The raw EEG signal, after manually excluding artifacts, was split into 10 s epochs for fast-fourier transformation (FFT) to generate power bands. The spontaneous recurrent CS were identified based on the EEG, power spectral characteristics, and video recordings for behavior (8). The mean plus/minus standard error values were pooled from 10 s epochs for spike counts, the average spike frequency per day was calculated for the first four weeks of post-SE, and the values were compared between the mild and the severe groups using two-way analysis of variance (ANOVA).

3.4. Morris Water Maze test and quantification
3.4.1. Fixed platform cue learning in Morris water maze

We used Morris water maze to evaluate the hippocampal dependent spatial learning and reference memory (27, 28) for mice that had mild or severe SE to test the effects of seizures on spatial navigation. The apparatus consisted of a galvanized stock tank of 1.15 meters in diameter filled with clear tap water maintained at room temperature before starting the tests. A clear circular plexi glass cylinder with a diameter of 11.2 cm was used as a platform. Two identical cues were used in this study: one cue was positioned directly above the platform zone (referred as "right cue") and the second cue was positioned in the zone without platform (referred as "false cue"). Both cues were placed constantly at the same place throughout all the trials. Both cues were raised 15 cm above the water level to maintain visibility for the swimming mice. A non-toxic white colored tempera paint was used to make water opaque to mask the platform during the submerged trials. When the platform was submerged, it was 1 cm below the water level, sufficient for mice to stand and raise above the water level. The mice were trained or tested at a fixed
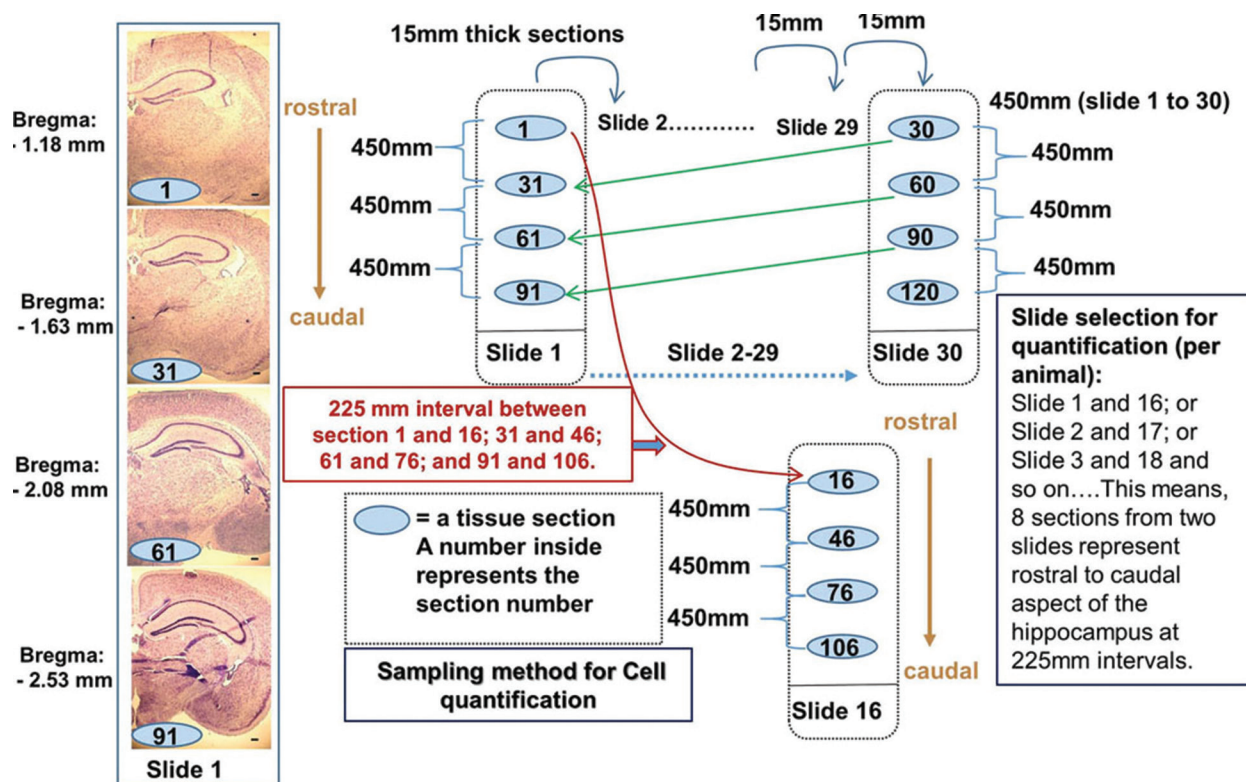
Figure 1. The method to sample the coronal brain sections, at 225 micrometer intervals, to represent the hippocampus from rostral to caudal for cell quantification. The 15µm serial sections (starting from rostral most part of the hippocampus- approximately at -1.1.8mm from Bregma, about 120 sections per mouse brain) were thaw mounted onto 30 slides sequentially in four rows starting from slide 1 to 30, as shown in the schematic diagram. The first 30 sections were placed on the first row of each slide serially followed by the 2nd, the 3rd and the 4th row. This method of sampling yielded sections on a single slide, separated by 450µm apart between sections, with a representative regions of the hippocampus, the entorhinal cortex and the amygdala from rostral to caudal. For example 1st and 31st sections, on the slide 1 are 450 micrometer apart represent the anterior region, the 61st section on the same slide represents the middle region, and the 91st section represents the posterior region of the hippocampus. A panel of photomicrographs of histology sections stained with cresyl violet and their approximate location from the Bregma is given on the left side of the images. For immunostaining, at least two slides (for example, slide 1 and 16) were selected in such a way that the gap between the corresponding sections on each slide is about 225 micrometers. For example, the distance between the 31st section on the slide number 1 and the 46th section on the slide number 16 is 225 micrometers. The immuno-positive cell counts were carried out on all 8 sections bilaterally from two slides per animal and the average number of immuno-positive cells were calculated per animal. Scale bars, all 100 microns.

time during the day. Five trials were conducted per day during training and each mouse had at least a 30-45 min gap between trials in a single day. The mice had the same starting position for each trial during the training period or submerged trials and later, the starting position was randomized for the subsequent trials on that day. A single probe trial was performed keeping a constant starting position for all mice. The mice were constantly monitored during the experiments. The video acquisition and analysis were performed using Any-Maze software (Stoelting Company, USA). For those mice which were unable to identify the platform within a minute were gently placed on the platform for 30 seconds after each test.

3.4.2. Training

The three groups of mice, 16 mice from the control group and 6 mice each from the mild and the severe SE groups, were trained for 5 days in Morris water maze. The training was started at 7d post-SE (day 1) to test the effects of seizures on learning and memory. On day 1, the mice were trained to identify the exposed platform (0.5 cm) above the water level. Five trials, each trial lasting for one minute, were performed per mouse on day 1. "The right and the false cues" were presented at the same position at all times in the clear and transparent water during the training period. These zones (true and false platform zone) had a diameter equivalent to the diameter of the plexi glass platform was considered for time spent during average of 1minute trials (Figure 11C). The training was repeated on day 2 (i.e., 8d post-SE) but with the platform was submerged under the clear water. From day 3 to 5 (i.e., 9-11d post-SE), the mice were trained similarly but in the opaque water to identify the submerged platform, as did on the day 2 training. The right and the false cues were maintained at the same position as in day 1 and 2 training. We chose 8 random starting points (such as east, west, north, south, north-east, north-west, south-east, south-west) around the

periphery of the tank during the training period as did on the day 1.

3.4.3. Probe trial

A single probe trial of one minute/mouse was performed on day 6 (12d post-SE) in opaque water. The platform was removed but the right and false cues were left at the same position. A random starting position was selected for the mice for the probe trial too, and they were allowed to swim for one minute to identify the right or false cues. The amount of time spent (in seconds) during the one minute probe in the "right cue zone or true platform zone" and the "false cue zone or false platform zone" were calculated for each moue. Any-Maze mice tracking software was used to calculate the time spent by each mice (in seconds) at the right cue or false cue zones during training periods (average values of all trials conducted per day) or during single probe trial. Since we chose random starting points for training and probe trials, we did not consider the path efficiency parameter in this study. Prior to the second probe trial on day 20 post-SE, the mice were re-trained on day 19 in the submerged platform (1 trial in clear water and 4 trials in opaque water). The results were recorded and quantified as we did for the previous trials.

3.5. MRI and quantification

T2-weighted MRI scans of coronal and horizontal planes were acquired from the sham control and epileptic mice, at 18 weeks post-SE, under isoflurane anesthesia using a small bore MRI system (Varian Unity/Inova 4.7. T, Varian Inc. CA) at the University of Iowa. The slice thickness (spacing) for imaging was 300 microns and had a depth of 16 bit. The images were analyzed using image-J (29). The ratio of area in pixels outlining both hippocampi with their respective cortex were determined for each sections to analyze the volume changes. The ratio of the area of the hippocampi to the cortex was determined for each coronal section of the MRI image of a mouse. An average ratio of the hippocampi to the cortex for each mouse was determined. The changes in the average ratios between the control mice, the mild SE and the severe SE groups were compared using Mann-Whitney test.

3.6. Tissue processing for histology and IHC

The brains were collected soon after perfuse fixation, post-fixed with 4 percent PFA for 4h at 4°C, and were gelatin-embedded as described previously (30, 31). The coronal sections (15µm) were cut on a cryostat (Cryostar NX70, ThermoScientific, MA, USA), and thaw-mounted sequentially onto chrome-alum-gelatin coated slides in such a way that each slide had four sections, 450µm apart, to represent the hippocampus, entorhinal cortex and amygdala from rostral to caudal aspect. This method of sampling for rat hippocampus has been described previously (32). A modified version of tissue sampling for mouse brain, to obtain sections at 225µm

intervals, and slide selection for quantification after immunostaining are illustrated in the Figure 1.

The brain sections for NeuN, GFAP, IBA1 and DCX were processed for double or triple IHC as described previously (31). Omission of primary antibody step served as a negative control for all antibodies, while morphology of neurons and their known location or glial cells morphology served as internal positive controls (e.g. profusely branched astrocytes irrespective of their reactive or normal state for GFAP; pyramidal neurons in CA regions of the hippocampus and granule cells of the dentate gyrus for NeuN). Following overnight incubation with the primary antibodies at 4°C, the sections were washed with PBS and treated with appropriate secondary antibodies (biotinylated or CY3/FITC conjugated) for 1h at room temperature. After further washes, the sections that were incubated with the biotinylated anti-species and later treated with streptavidin-CY3 (1:300 for CY3 and 1:100 for FITC, Vector Laboratories, USA) for 1h, washed thoroughly in PBS, rinsed in distilled water to prevent salt crystal deposits on sections, and cover-slipped with vectashield-with DAPI® (Vector Laboratories, USA). The sections were viewed under the Zeiss inverted microscope (Axiovert 200) and photographed with Hamamatsu digital camera (Model C-10600-10B) using HCImage live (version 4.1.2.) software. For cell quantification, photographs were taken at 20x magnification (10x for Figures) keeping exposure time constant for all images.

In order to identify degenerating neurons in the hippocampus, the entorhinal cortex, and the amygdala the brain sections were processed for NeuN and FJB double staining. The sections were first stained for NeuN antibody as described above. Later, these sections were processed for FJB staining using a modified protocol from previously published method (11, 33-35). The sections on the slides were rehydrated sequentially in descending grades of ethanol starting with 100 percent for 3 min, followed by a 1 min each in 70 percent ethanol and distilled water. The slides were then transferred to 0.06 percent potassium permanganate solution for 10 min with slow shaking. After rinsing with distilled water for 1 min, the slides were transferred to 0.004 percent FJB (Histo-Chem Inc., AR) in 0.1 percent acetic acid for 30 min with slow shaking in dark. The sections were later rinsed three times in distilled water and air dried in dark for 4h. Later the sections were dehydrated in ascending grades of alcohol, cleared in xylene, and mounted with distyrene plasticizer xylene (DPX, Electron Microscopy Sciences, PA) or acrytol (Surgipath, Leica biosystems, IL) mounting medium.

3.6.1. Immunopositive cell quantification

Procedure for cell counting has been described in our previous publications (30, 31, 36). ImageJ software (29) was used to measure the counting area (square microns) and the person counting cells was blind

to the experimental groups. The cell counting area from each section was kept constant for all the experimental groups and controls. Bilateral counts were made from a minimum of eight sections per animal as described previously (30-32). The NeuN was used to mark neurons and the average number of neurons expressing FJB in each region was calculated. Microglia (IB1A), astrocyte (GFAP), and neuroblast (doublecortin (DCX)) cell markers were counterstained with DAPI and only those cells positive for cell marker and with a visible nucleus were counted from CA regions of the hippocampus, the dentate gyrus, the entorhinal cortex and the amygdala. The normal and reactive glial cells were distinguished based on their morphology.

3.7. Statistics

The average (mean plus/minus standard error) numbers of immuno-positive cells from 8 sections from 2 slides containing anterior, middle and posterior regions of the brain were calculated for each mouse within the group. To derive statistical differences (p less than 0.05) between the groups, Mann-Whitney test was applied. Likewise we compared the group performance in Morris water maze, and volumetric parameter from MRI images.

4. RESULTS

4.1. The epileptiform spike rate and the frequency of spontaneous CS increase with the severity of SE during the first two weeks after the SE

As described previously, the behavioral cumulative seizure severity index during the SE was used to classify the mice as the mild or the severe SE group (8, 9). Our previous studies have demonstrated that both mild and severe SE induce immediate epileptogenesis, however the only difference was that the severe group experienced more numbers of spontaneous recurrent CS during the first four weeks of the SE (8). We further extended this study to quantify and compare the epileptiform spiking during the first four weeks between the two groups. Following termination of the behavioral SE with diazepam, no behavioral seizures were observed during the first 18 hours, however the electrographic NCS and epileptiform spiking continued to persist (Figure 2). The spontaneous behavioral CS and electrographic NCS, and interictal epileptiform spikes were present throughout the 28 days in all the mice irrespective of the severity of SE. There were about 16 plus or minus 3 (Mean plus or minus SEM) spontaneous CS in 4 weeks in the severe group and about 4 plus or minus 1 in the mild group. The spike frequency per minute (spike rate) was significantly higher in the severe group during the first 12 days post-SE when compared to the mild group (Figure 3, p=0.0007, Two-way ANOVA, F=11.89 with 1-140 degrees of freedom). However, after the day 12 the spike frequency was less than 5 spikes/minute in both groups.

4.2. Electrographic features of epileptogenesis: Characteristics of post-diazepam EEG, pre-, post-, inter-ictal spikes, and NCS clusters during the first two weeks of post-SE

In the mild or the severe SE group, after diazepam administration, the behavioral seizures stopped. The electrographic seizures persisted although the amplitude of the epileptiform spikes reduced briefly (Figure 2B, a) during the first 20-30 minutes and reached the basal level by 16h (Figure 2A). We classified the non-convulsive interictal spikes and or episodes, and convulsive episodes based on the individual spike characteristics observed during the SE (8, 9). After the first 3h post SE, the high amplitude epileptiform spikes (predominantly stage-2 spikes) began to appear in trains lasting for 15-30 minutes with an interspike intervals of 0.3-3 seconds (0.3-3 hertz, Hz, Figure 2B, a). The stage-2 spike trains started clustering by 6 hours (Figure 2B, c). Thereafter, stage-1 epileptiform spiking (0.2 -0.6 Hz) emerged along with stage-2 spike activity (Figure 2B, d). Later, stage-1 started to appear independently as "a string of pearls" referred to as stage-1 non-convulsive episodes (Figure 2B, e). The spiking pattern subsequently developed into a high amplitude stage-2 non-convulsive episodes with an increase in their duration (15-25s episode duration, Figure 2B, f). By 7d post-SE non-convulsive episodes gradually evolved to culminate in stage-3 CS episode (Figure 2B, g). By 14d post-SE, several stage-3 convulsive episodes occurred before the stage-5 CS episode (Figure 2B, h).

4.3. Impact of epileptiform spiking and spontaneous CS on brain pathology at 7, 14 and 28 day post-SE

We quantified reactive gliosis to investigate time-dependent effects of the mild and the severe SE in the hippocampus, entorhinal cortex, and amygdala at 7, 14, and 28 days. Reactive astroglia and microglia were identified based on IHC using GFAP and IBA1 as cell markers for astroglia and microglia cells, respectively. The reactive astrocytes were characterized by thick cytoplasmic processes with intense GFAP staining (Figure 4). We have previously shown that both reactive astrogliosis and microgliosis occurs as early as three days post-SE in the C57BL/6J mouse kainate model (31). The reactive astrogliosis and microgliosis were found in and around the cornu ammonis-3 (CA3) region of the hippocampus at 3d post-SE (31). In the present study, a similar pattern but more diffused reactive astrogliosis was observed in all CA regions of the hippocampus, the hilus and the molecular layers of the dentate gyrus at all the time points (Figures 4). There was a significant increase in reactive astrogliosis in both the mild and the severe SE groups at 7 day when compared to the control in CA1, CA3 and dentate gyrus (Figure 4B, p less than 0.05, Mann-Whitney test). Further, severe SE group had significantly higher numbers of reactive astroglia cells at
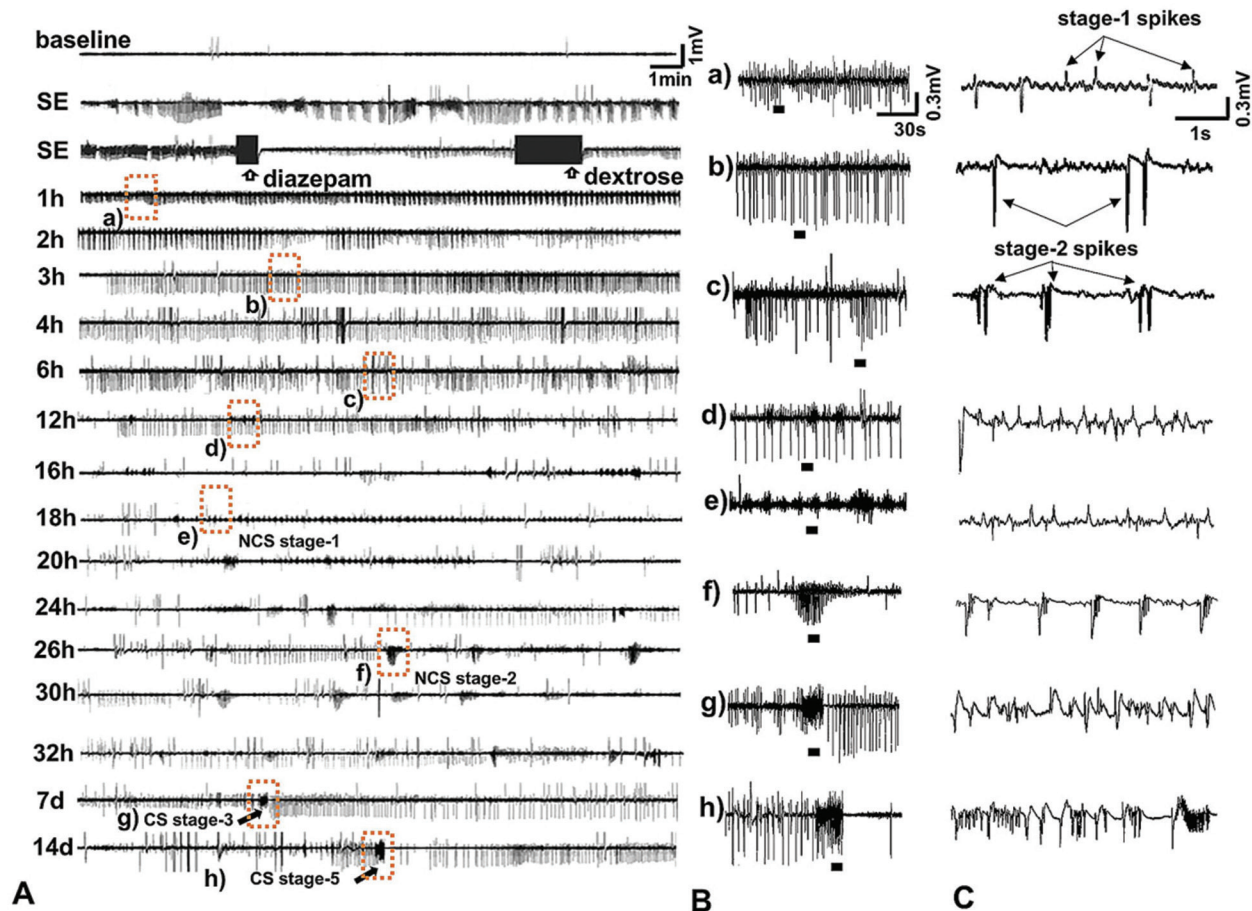
Figure 2. Representative EEG traces from a severe group mouse after terminating the behavioral SE with diazepam, and during the first 14 days of post-SE period. Each EEG trace in panel A represents 20min of duration. The panels in B represent the expanded 2 min EEG traces shown in the boxes in A. The black bars below the EEG traces in B is further expanded as 5second traces in C. The SE was terminated by diazepam 2h after the onset of stage 3 (mild) or stage 5 (severe) seizure and dextrose normal saline injection was given thereafter. Although behavioral seizures stopped, epileptiform spikes continued to occur. These spikes organized into distinct patterns during epileptogenesis before developing into spontaneous recurrent convulsive seizures by 7d (stage-3) and by 14d (stage-5). The electrographic events during epileptogenesis include: (i) a transient decrease in the amplitude of epileptiform spiking soon after the diazepam injection (seen in trace 'a') (ii) initiation of newly formed epileptiform spike trains (seen in the trace 'b') (iii) progression of spike trains into spikes clustering (seen in the traces 'c' and 'd') leading to evolution of spontaneous recurrent NCS (as seen in the trace NCS stage-1 in 'e' and NCS stage-2 in 'f'). (iv) first spontaneous recurrent CS (stage 3, seen in the trace 'g') occurred on day 7, and (v) after several episodes of stage 3 CS, a first spontaneous recurrent CS stage-5-5 developed (as seen in the trace 'h').

both 7d and 14d time points when compared to the mild SE group (Figure 4B, p less than 0.05, Mann-Whitney test). Likewise, reactive astrogliosis was also observed in the entorhinal cortex and the amygdala (Figure 5; p less than 0.05, Mann-Whitney test, n=5).

The reactive microglia cells were also quantified based on their morphology. They were hypertrophic and had a few thick but short cytoplasmic processes resembling pseudopodia and often amoeboid with several nuclei (Figures 6A and B) (37, 38). The reactive microglial cells were concentrated in and around the pyramidal cell layers in the CA3 and CA1 regions more frequently in the severe group than in the mild group at 7d post-SE (Figures 6A and B). In the severe SE group, the microglial cells were large and contained several nuclei suggesting their phagocytic nature, and their processes

were frequently found to surround the NeuN positive cells (Figure 6B, iii, Z). The number of NeuN positive cells were fewer around the vicinity of the reactive microglial cells at 7d post-SE (Figure 6B, Z). The reactive astrocytes were also frequently found in the stratum pyramidale where the neurons were missing (Figure 6B, W, Z). The reactive microglia counts were also higher in the severe SE group than in the mild SE group at 7d, but not at 14d time point (Figure 6C, p less than 0.05, Mann-Whitney test). A similar pattern of increased reactive microgliosis at 7d post-SE was also observed in the entorhinal cortex and the amygdala (Figure 7).

Overall, the reactive astroglia and microglia cell counts significantly reduced in both the severe and the mild groups after 7d time points in the hippocampus (p< less than 0.05, Mann-Whitney test, n=5), the
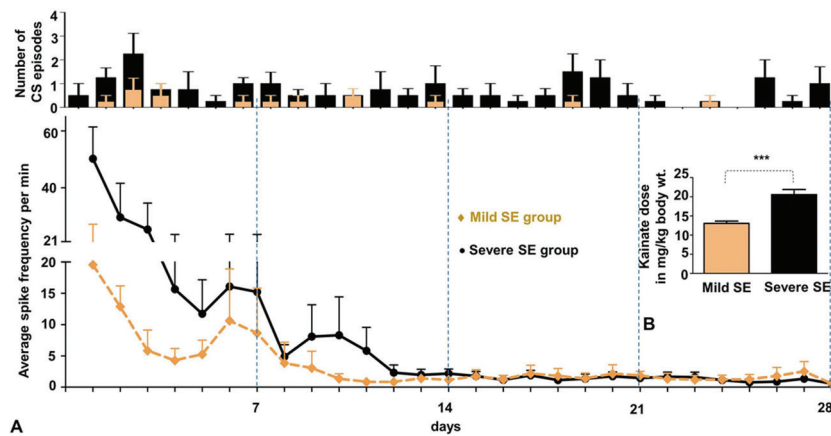
Figure 3. Comparison of the average epileptiform spike frequency in 1 day epochs during the first four weeks after the SE in the mild and the severe groups. A. The severe SE group had a higher spike frequency during the first 12 days and reached to the same level as the mild group thereafter (p=0.0007, Two-way ANOVA, F=11.89 with 1-140 degrees of freedom, n=4). A bar graph above shows the number of CS episodes/day in mild (n=4) and severe (n=4) SE groups. B. An inset bar graph showing a significant difference between the amount of kainate received by the mild and the severe SE groups (p=0.0.001, n=16 each, Mann-Whitney test) to achieve stage 3 or stage 5 seizures, respectively, during the SE. On an average, the mild SE group mice required 3 doses of 5mg/kg to achieve stage less than or equal to 3 seizures, while the severe group required 4-5 doses to achieve stage-5 seizures.
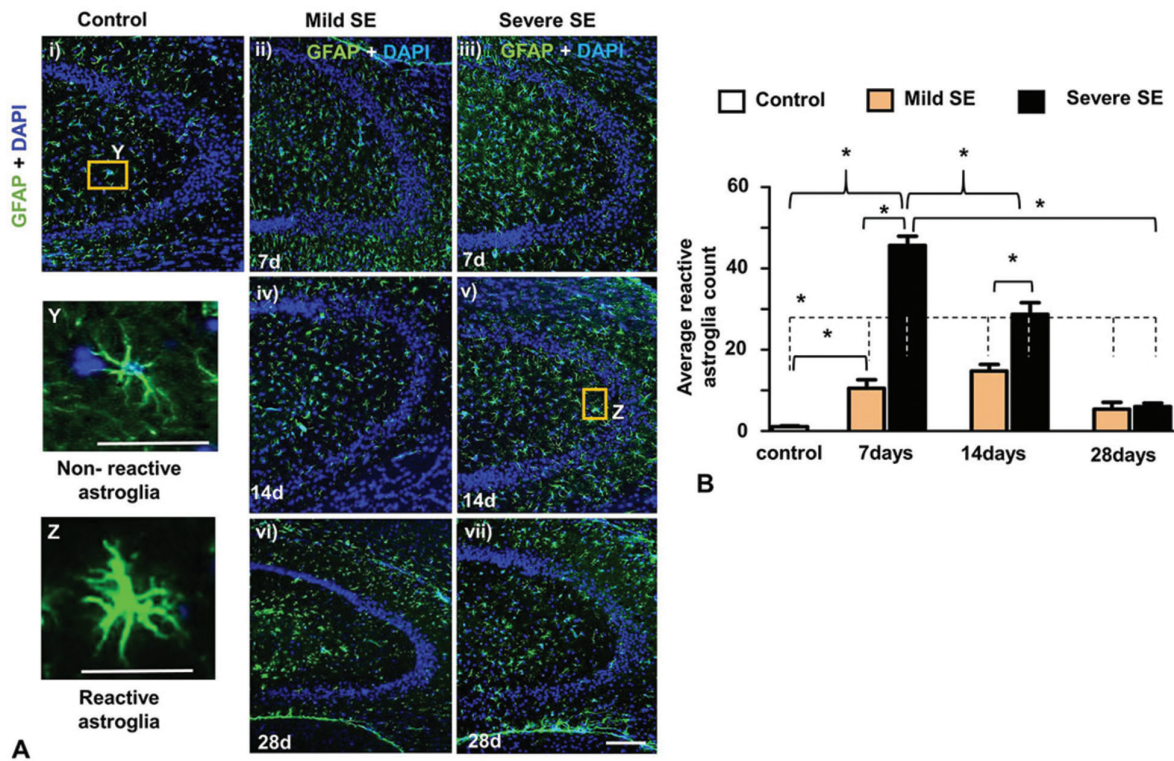
Figure 4. Reactive astrogliosis in the severe and the mild SE groups at 7d, 14d and 28d time points in CA3 region of the hippocampus. A. 10x magnified photomicrographs showing GFAP positive astrocytes (green; DAPI for nucleus, blue). Representative magnified images of normal (boxed in the panel 3Ai, marked as Y) and reactive astrocytes (boxed in the panel 3Av, marked as Z) are shown separately (Y and Z). Scale bars, all 100 microns. B. The reactive astrocytes in and around the stratum pyramidale were counted from CA regions of the hippocampus and the dentate gyrus at all three time points. There were significantly higher numbers of reactive astrocytes in the severe SE group at 7d and 14d post-SE when compared to the mild SE and the control groups (n=4 each, *p=0.029 control vs 7d mild, *p=0.029 control vs 7d severe, *p=0.028 mild vs severe 7d groups, *p=0.0294 mild vs severe 14d groups, Mann-Whitney test). There was significant reduction in reactive astrogliosis in the severe group from 7d to 28d time points (*p less than 0.05, severe 7d vs 14d and 7d vs 28d, 14d vs. 28d, Mann-Whitney test). The reactive astrogliosis was reduced at 28 day post-SE, but were significantly higher in both groups when compared with the control (*p=0.0286, control vs. mild 28d, and control vs, severe 28d, Mann-Whitney test).
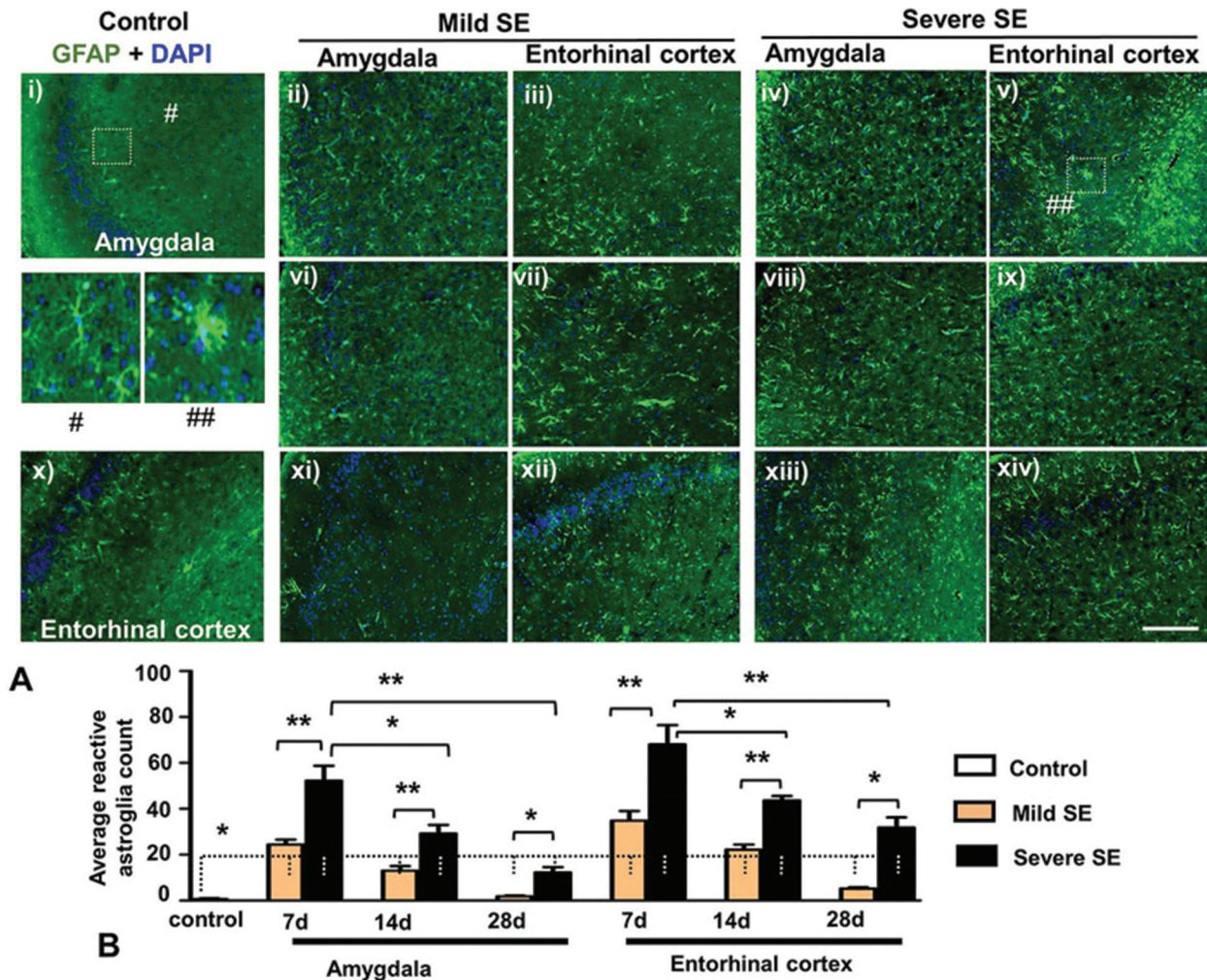
Figure 5. Reactive astrogliosis in the entorhinal cortex and the amygdala of the severe and the mild SE groups at 7d, 14d and 28d post-SE time points. A. 10x magnified photomicrographs showing GFAP positive astrocytes (green; DAPI for nucleus, blue). B. Cell quantification. The reactive astroglia significantly increased in both the mild and severe groups when compared to the naïve controls at all the time points (p less than 0.05, Mann-Whitney test, n=5 each). The severe SE group had significantly higher reactive astroglia compared to the mild SE group at all time points, however a significant reduction in their numbers was observed at 14d and 28d time points when compared to 7d post SE (p less than 0.05, Mann-Whitney test). Magnified images of astrocytes shown in # (normal) and ## (reactive astrocyte). Scale bars, all 100 microns.

entorhinal cortex (p less than 0.05, Mann-Whitney test, n=5) and the amygdala (p less than 0.05, Mann-Whitney test, n=5). However, when compared to the control, there was a persistent increase in reactive astrogliosis at all three time points and in all three brain regions, while the reactive microglial cell counts reached the basal level by 28d post-SE (Figures 6C and 7B).

At 7 day post-SE the reactive microglial cells continued to dominate the CA3 and CA1 regions of the hippocampus (Figures 6A and B), the entorhinal cortex and the amygdala (Figure 7A). This observation, coupled with increased brain electrical activity (Figure 2 and 3) at this time point, prompted us to investigate whether neurodegeneration occurred during this period. FJB+NeuN staining revealed significant

neurodegenerative changes in the same areas where there were a large numbers of reactive microglial cells. A large numbers of FJB positive cells were found in the hippocampus, the entorhinal cortex and the amygdala at 7 and 14 days in both the severe and the mild groups when compared to the control (Figures 6 and 8). However, at 28d their number declined in both groups, in all three regions, when compared to the 7d post-SE (Figures 6D and E, 8) which were similar to the patterns observed in reactive microglia and astroglia cell counts (Figures 4B and 6C).

Having observed dramatic changes in reactive microglia and astrocytes, and neurodegeneration at 7 and 14 days, and recovery, to some extent, by 28 days in all three brain regions, we focused our investigation on
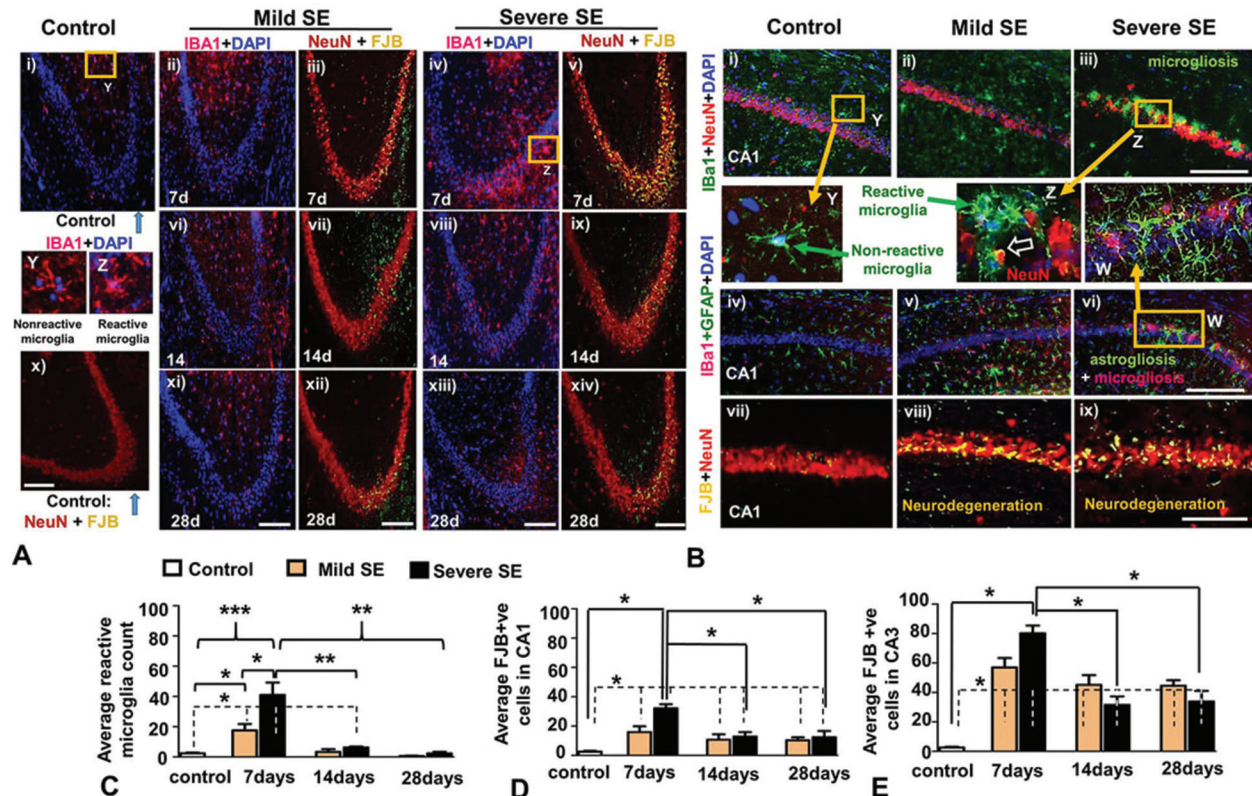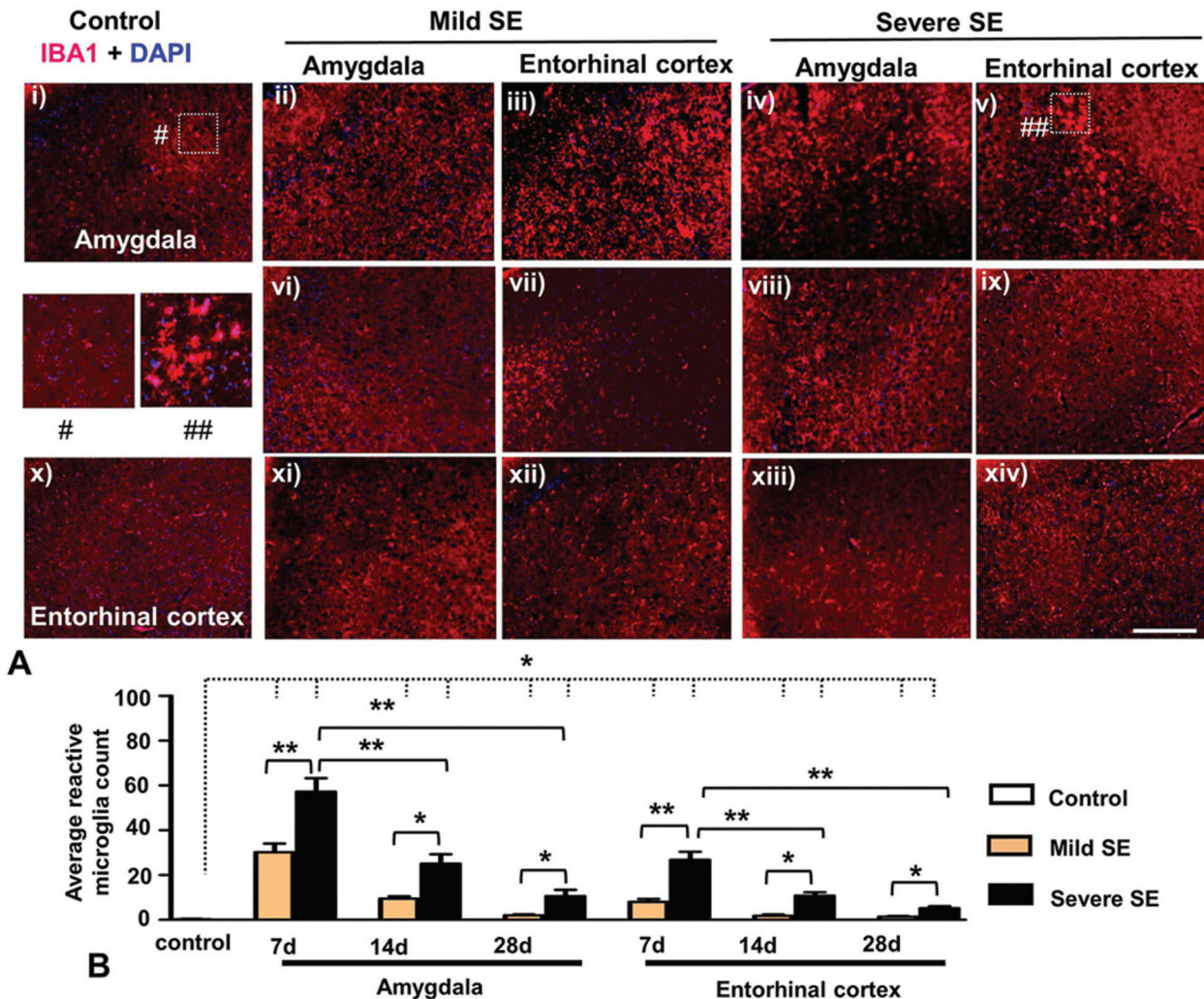
Figure 6. Reactive microgliosis and neurodegeneration in the hippocampus in the mild and the severe SE groups at 7d, 14d and 28d time points. A. 10x magnified photomicrographs showing IBA1 positive microglial cells (pink cells) containing nucleus (DAPI, blue). The reactive microglial cells were concentrated more in and around the stratum pyramidale at 7d in the severe group (iv). A magnified images of normal (boxed in i) and labeled as Y) and reactive microglia (boxed in iv and labeled as Z) are shown in the panel Y and Z, respectively. The slides containing adjacent brain sections (with 225 micrometers apart) were processed for NeuN+FJB immunostaining to reveal neurodegeneration. At 7d post-SE in the severe SE group, the NeuN+FJB positive neurons were concentrated in the CA3 region (v) where the reactive microglial cells were also present (iv), and these changes were moderate at 14d (viii, ix) and 28d (xiii, xiv). In the mild SE group, reactive microgliosis and neurodegeneration were mild at 7d post-SE and they decreased further later on (ii and iii; vi and vii; xi and xii). Scale bar, all 100 microns. B. The photomicrographs presented in B are from CA1 region- taken from the same sections as in the panel A from 7d post-SE group. The CA1 hippocampus too showed hypertrophied phagocytic reactive microglia (green cells in iii; the red cells are NeuN positive) in the severe SE group. The boxed area in (iii) is enlarged to show the morphology of reactive microglia cells that contain several nuclei (panel Z) when compared to the normal microglia from the control (i, the boxed area is enlarged- panel Y). Reactive microglia cells frequently wrapped the NeuN positive neurons (red, indicated by an open arrow in the panel Z). The parallel sections were also double stained for IBA1 and GFAP to understand the relationship between microglia and astrocytes at the site of neurodegeneration. The GFAP positive reactive astrocytes (green, iv to vi, and W) were frequently observed in close proximity with the reactive microglia cells (pink, iv to vi, and W) with no NeuN positive cells around (perhaps engulfed by reactive microglia) suggesting the neuronal loss in that area. Those neurons undergoing degenerative changes were stained for FJB and NeuN (yellow stained cells in the panel vii to ix). The healthy neurons were stained by NeuN only. Those cells that stained for both FJB and NeuN were counted from CA1 and CA3 region of the hippocampus. Scale bar, all 100 microns. C-E. Cell quantification. There were significantly higher microglia cell counts in both the mild and the severe SE groups at 7d post-SE when compared to the control group (*p=0.017 control vs mild 7d, ***p=0.0006 control vs severe 7d, *p=0.0.38 mild vs severe 7d groups, Mann-Whitney test, n=5 each). The reactive microgliosis significantly reduced at 14 and 28d time points in the severe groups when compared to the 7d time point (**p=0.0028 severe 7d vs 14d and severe 7d vs 28d, Mann-Whitney test). There were significantly higher numbers of FJB positive cells in both CA1 (D, *p=0.0286, control vs severe 7d or severe 14d or severe 28d, Mann-Whitney test, n=4 each) and CA3 (E, *p=0.0286, control vs severe 7d or 14d or 28d, Mann-Whitney test, n=4 each) regions at 7, 14 and 28d post-SE in the severe groups when compared to the controls. There was a significant difference between controls and 28d mild group at CA1 and CA3 regions (*p=0.0286, Mann-Whitney test). However, there was a significant reduction in the number of FJB positive cells in the severe SE group at 14 and 28d time points when compared to 7d time point at CA1 and CA3 regions (*p=0.0286, severe 7d vs 14d or 28d, Mann-Whitney test, n=4 each).

the dentate gyrus. At 7d post-SE, we observed reactive astrogliosis in the hilus with thick (GFAP positive) astrocytic processes penetrating through the dentate granule cells in both the mild and the severe groups (Figures 9A and 10A). The NeuN immunostaining revealed a significant reduction in the number of hilar neurons in both the mild and the severe SE groups at 7d post-SE when compared to the control group (Figure 9B). The NeuN+FJB double staining of the adjacent sections revealed that a large

numbers of hilar neurons were FJB positive in both the mild and the severe groups suggesting an increase in neurodegeneration in the hilus of the dentate gyrus (Figure 9C; p=0.0286, Mann-Whitney test). At 14 and 28 days their numbers were reduced, the similar trend as for the reactive gliosis (data not shown).

Interestingly, in both the mild and the severe groups we found a large numbers of DAPI positive
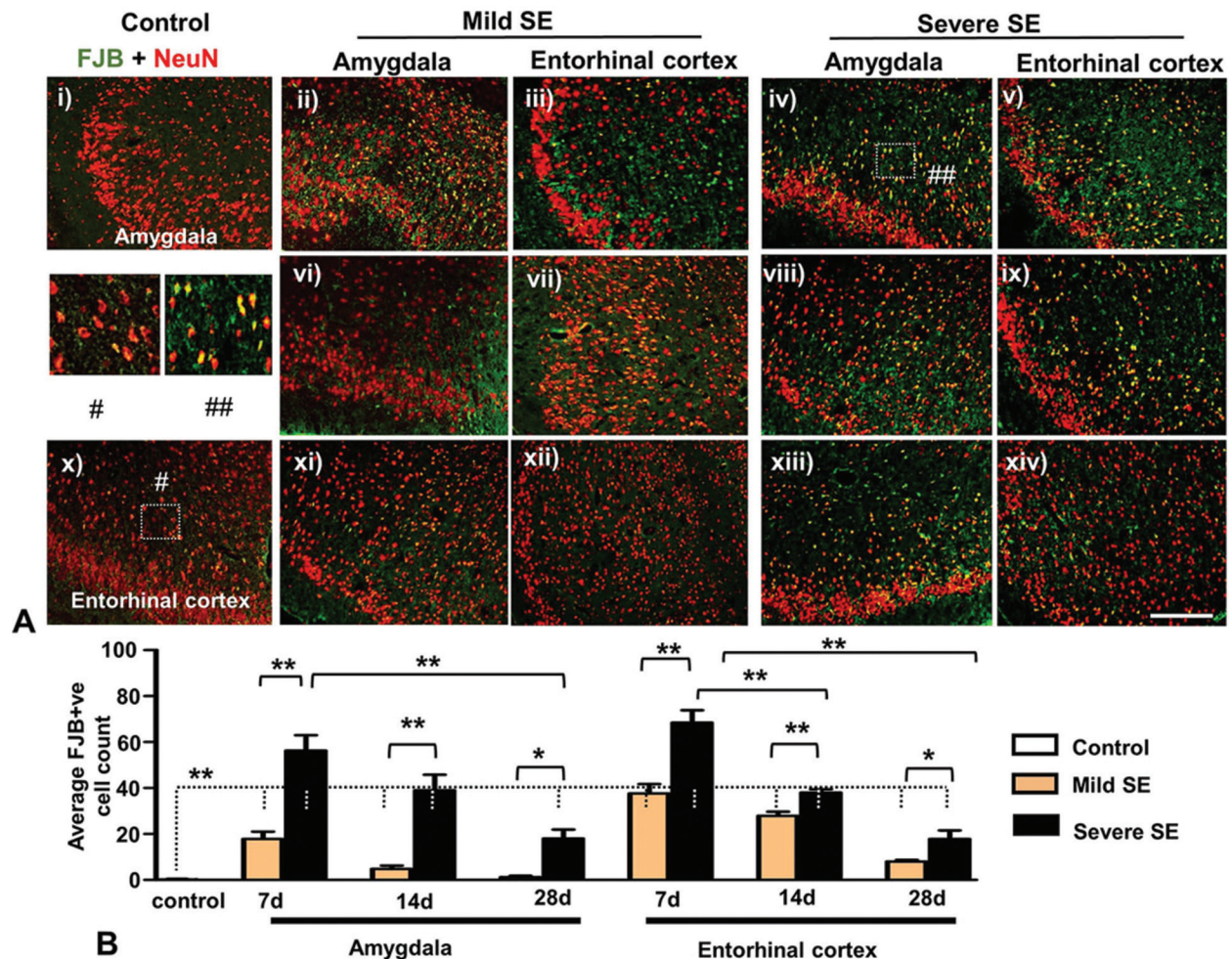
Figure 7. Reactive microgliosis in the entorhinal cortex and the amygdala of the severe and the mild SE groups at 7d, 14d and 28d time points. A. 10x magnified photomicrographs showing IB1A positive microglia (red; DAPI for nucleus, blue). B. Cell quantification. The reactive microglia significantly increased when compared to the naïve controls at all the time points (p less than 0.05, Mann-Whitney test, n=5 each). The severe SE group had significantly higher reactive microglia compared to the mild SE group at all time points while a siginificant reduction was observed at 14d and 28d time points when compared to the 7d post-SE groups (p less than 0.05, Mann-Whitney test). Magnified images of microglia shown in # (normal) and ## (reactive microglia). Scale bars all 100 microns.

cells that were neither positive for NeuN nor for GFAP in the subgranular zone (SGZ) of the dentate gyrus (Figure 9A). Based on our previous observation in the rat kainate model (32), we predicted that these cells could be neuroblasts. A double cortin (DCX) immunostaining was done to confirm this (Figure 10A). When compared with the control, the cell counts revealed a significant increase in the number of DCX positive cells in the SGZ at all the time points in both the mild (except at 28d) and the severe SE groups (Figure 10B). In the granule cell layer too, the DCX positive cells were higher at 7d and 14d when compared to the control in both the mild and the severe groups. In the hilus, such increase was found at 7d in the severe group only (Figure 10B). However, by 18 weeks, MRI revealed no significant changes in the

ration of volume of the hippocampus to the rest of the volume of the brain in the severe and the mild groups or when compared to the control group (Figures 10C and D). Further, cresyl violet staining of brain sections of mice that had persistent electrographic NCS for 18 weeks (evident from continuous video-EEG recording) did not reveal significant differences in morphological changes between the groups (data not shown).

4.4. Impact of epileptiform spiking, spontaneous CS and electrographic NCS, and brain pathology on hippocampal dependent discriminatory learning and memory

The Morris water maze test was performed to investigate the effects of the severity of seizures on

400

Figure 8. Neurodegeneration in the entorhinal cortex and the amygdala of the severe and the mild SE groups at 7d, 14d and 28d time points. A. 10x magnified photomicrographs showing FJB and NeuN positive cells (yellow; Green- FJB, red- NeuN, DAPI for nucleus, blue). B. Cell quantification. The number of FJB positive cells significantly increased when compared to the naïve controls at all the time points except 28d time point in amygdala (p less than 0.05, Mann-Whitney test, n=5 each). The severe SE group had significantly higher FJB positive cells when compared to the mild SE group at all time points while a siginificant reduction in their number was observed at 14d and 28d time points when compared to the 7d post-SE groups (p less than 0.05, Mann-Whitney test). Magnified images of neurons shown in # (normal) and ## (FJB positive neurons). Scale bars all 100 microns.

discriminatory learning and memory. Considering the impact of the seizures on the hippocampus with respect to reactive gliosis, neurodegeneration, and neurogenesis, it was anticipated that the cognitive function could have been compromised in the epileptic mice. The mice were tested between 7-20 days post-SE, the period during which maximum pathology was observed. There were no differences between the control and the mild SE group with respect to the amount of time required to find the exposed platform on the day 7 (Figure 11A). However, the mild SE group mice spent more time at the false zone during the probe trails on day 12 and 20 post-SE suggesting the loss of memory. An interesting observation on the day 7 (training/learning trials) was that the severe SE group mice had a tendency to learn incorrectly i.e. they learned to choose the false zone instead of the exposed platform in contrast to the control and the mild

SE groups. The incorrect learning was further reinforced during the submerged platform trials (day 8-11 post-SE) and the probe trial at 12d post-SE. However, after a gap of 7 days there was an improvement in the correct learning (i.e. choosing the true platform zone) after a short training in the submerged platform trials in the severe group (p less than 0.05, Mann-Whitney test). The tracks of representative mice from each group travelled during the probe trail is presented in Figure 11C.

5. DISCUSSION

In the present study we demonstrate the effects of initial seizure severity during the SE and subsequent epileptiform spiking activity, in the C57BL/6J mouse kainate model, on the neurobiological changes in the hippocampus, the entorhinal cortex, and the amygdala
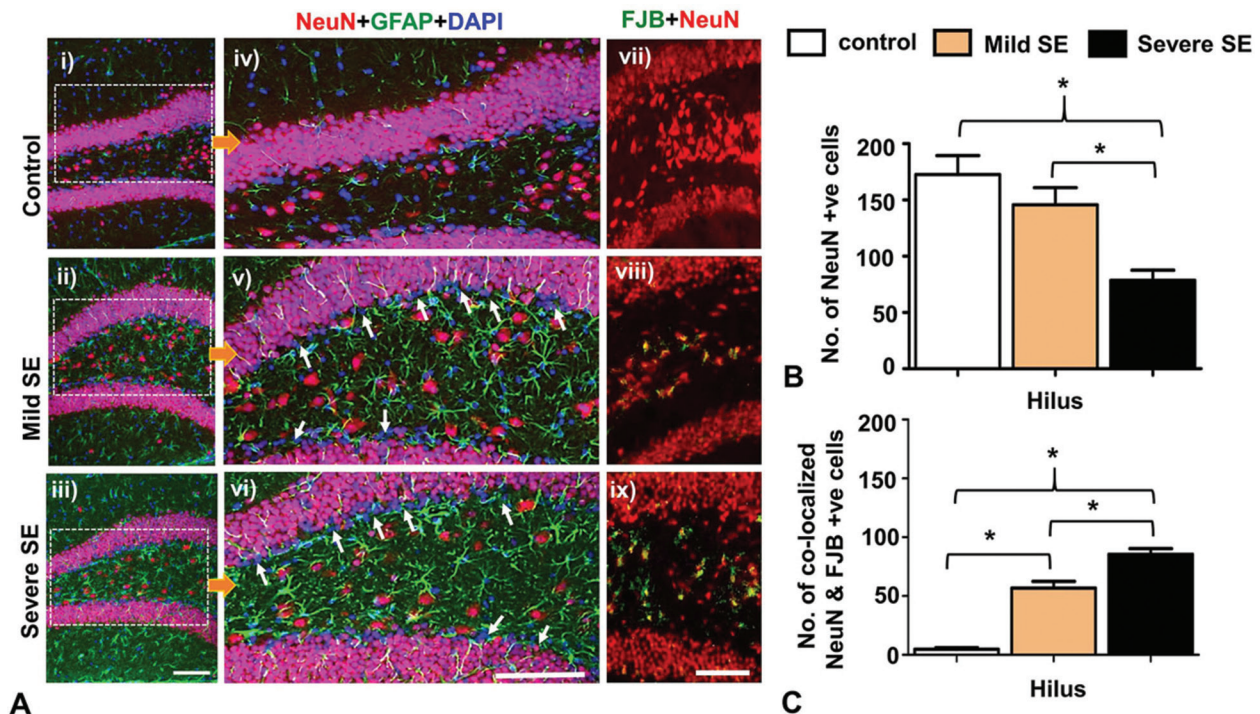
Figure 9. Neurodegeneration and reactive astrogliosis in the hilus of the dentate gyrus at 7d post-SE in the severe and the mild SE groups. A. 10x photomicrographs (i-iii) from 7d post-SE brain sections labeled for astrocytes (GFAP, bright green), neurons (NeuN, bright red/pink) and nucleus (DAPI labeled in blue). These images were further magnified in the panel iv-vi to show the subgranular zone and the cells in the hilus. The thick processes of the reactive astrocytes passing through the dentate granular cells were observed in both the groups. The white arrows in the panel v-vi (A) point to the subgranular zone are the DAPI positive cells that did not stain for NeuN or GFAP suggested that these cells were neither neurons nor astrocytes. These cells were DCX positive neuroblasts (shown in the Figure 10A). The NeuN (red) and FJB double stained neurons (yellowish green) in the hilus are shown in the panel vii-ix. Scale bar, all 100 microns. B-C. Cell quantification. There was a significant reduction in the NeuN positive cells in the hilus region in the severe SE groups when compared to the control or mild SE group when compared to severe SE (*p=0.0159, n=5, Mann-Whitney test). C. The graph showing an increase in co-localization of NeuN and FJB positive cells in the hilus in the mild SE and the severe SE groups when compared to the control (*p=0.0286, control vs mild, control vs severe, mild vs severe Mann-Whitney test, n=4 each).

during the early stage of epilepsy. The EEG recording and the IHC of brain sections from the mild and the severe SE groups revealed increased spiking activity with distinct pattern of EEG footprints of epileptogenesis, increased reactive astrogliosis and microgliosis, increased neurodegeneration and a concomitant increase in neurogenesis at 7 and 14 days post-SE. Most of these changes were reduced at 28 day post-SE. These early changes caused a significant reduction in the water maze performance in both groups indicating a cognitive decline during the early epileptic phase. Our findings from this study also seems to suggest that increased neurogenesis between 7-14 days and decreased reactive gliosis and neurodegeneration by 28 day may be responsible for reducing spontaneous CS after 4 weeks in the C57BL/6J mouse model of epilepsy. However at a longer time point (18 weeks post-SE), neither MRI nor histology (data not shown) showed any gross changes in the brain between the groups suggesting that a different mechanism exists for the persistent spontaneous NCS that were observed in both the mild and the severe SE groups (8).

The C57BL/6J mice are resistant to kainate-induced toxicity via the i.p. route (1, 2). Moreover their response to a single high dose of kainate was highly variable between different batches of mice and between different suppliers (8, 9, 39, 40). Also, an increased mortality rate was reported with a single high dose of kainate (normally greater than 20mg/kg, i.p.) (2, 5, 6, 41). To overcome variability in seizure response to kainate and to reduce mortality rate, we demonstrated an alternate method of repeated low dose of kainate (5mg/kg, i.p.) given at 30 minutes intervals (9). This method is useful to titrate mice to a varying degree of severity based on the Racine scale (26). This method induced immediate epileptogenesis irrespective of the severity of seizures during the SE (8). We also further demonstrated a method of quantifying severity of the SE (cumulative seizure severity indices) based on real-time behavioral seizures and their corresponding EEG characteristics (8, 9). In the present study, we compared the long term effects of severe and mild SE on the brain electrical activity, pathology and the functional outcome. The studies from McKhann *et al* (3) and Yang *et al* (4), using repeated dose of kainate at different concentrations and intervals in the C57BL/6J mouse model, also reported increased seizure severity and decreased variability in seizure response. Since these were short term studies, the long term impact
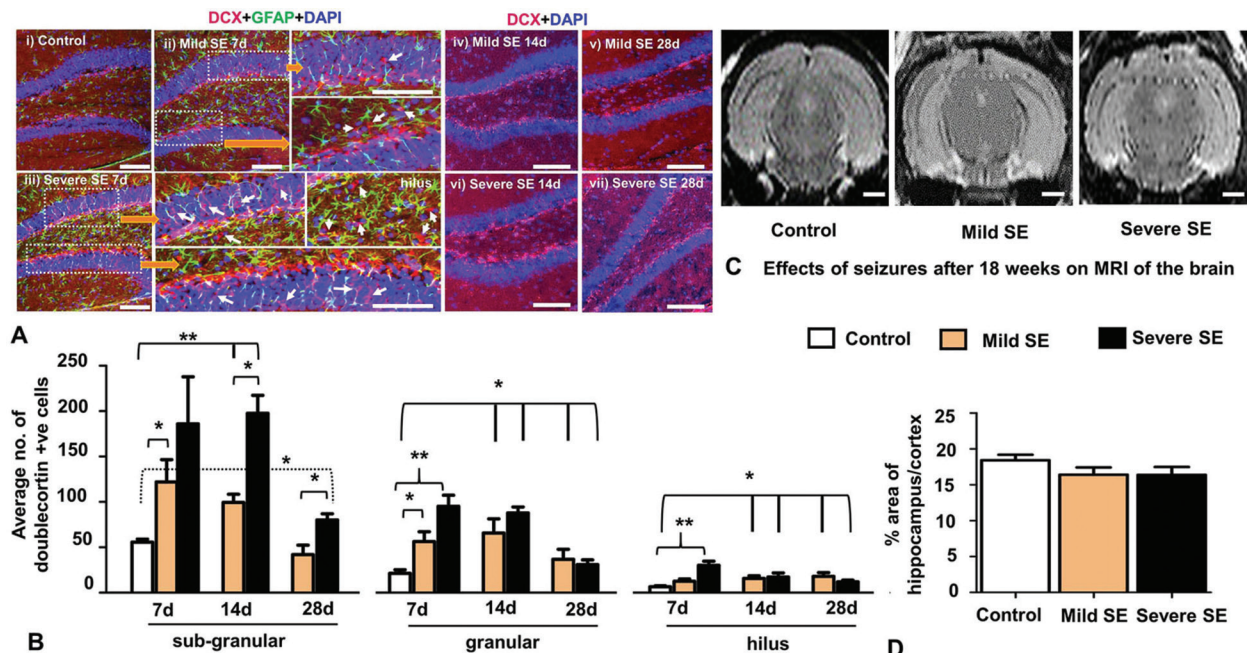
Figure 10. Neurogenesis at 7d, 14d and 28d post-SE in the severe and the mild SE groups and MRI at 18 week post-SE. A. The photomicrographs of the brain sections immunolabeled for astrocytes (GFAP, green) and doublecortin (DCX, pink/red), and counterstained with DAPI (blue). A further magnified images from ii) and iii), indicated by large orange arrows, to demonstrate DCX positive cells in the hilus, subgranular and granular zones. The panel iv) to vii) represent DCX staining in the dentate gyrus from the mild (iv, v) and the severe (vi-vii) at 14 and 28d post-SE. Scale bar, all 100 microns. B. Cell quantification. There was an overall increase in the DCX positive cells in the subgranular and the dentate granule cell layer, and the hilus in both the severe and the mild SE groups when compared to controls at all the time points (except at 28d time points and in the subgranular zone at 28d in the mild group) (*p less than 0.05, Mann-Whitney test, n=5). At 7d post-SE there was a significant increase in the DCX positive cells in the subgranular zone which were neither NeuN nor GFAP positive as shown in the Figure 9A. An increase in the DCX positive cells (indicated by white arrows in 7d post-SE group) in the granule cell layer suggest their migration from the subgranular zone, and also in hilus in the severe and the mild SE groups than the control (A- indicated by white arrows) (*p less than 0.05, Mann-Whitney test, n=5). There was an overall decreasing trend in DCX positive cells at 28d time point compared to other time points in all three regions of the dentate gyrus. C-D. The MRI images of the control, mild and severe SE groups at 18 week did not show any morphological or volumetric changes in the hippocampus. 1mm scale bar for all images in C.

of severity of SE on epileptogenesis and neurobiological changes in the brain were not reported. In our studies, in addition to quantifying behavioral and electrographic SE, we further quantified the EEG for epileptiform spike rate with EEG patterns of epileptogenesis during the first four weeks (Figure 2 and 3) and spontaneous CS and electrographic NCS for 18 weeks post-SE (8). The epileptiform spikes detected during the post-SE period resembled inter ictal spikes and periodic epileptiform discharges as described for the C57BL/6J mouse kainate model (25, 31) and the rat kainate model (42). Further, it has been demonstrated that the inter ictal spike frequency could be a strong predictor of chronic epilepsy (43). A similar observation was made from our present and the previous studies from the C57BL/6J mouse chronic model of complex seizures (8).

SE causes neuroinflammation as a delayed effect (8, 44-49). SE disrupts the blood-brain-barrier (BBB) irrespective of severity of seizures (4, 50-53). The loss of BBB integrity causes infiltration of leukocytes and serum albumin in the extracellular space and increases GFAP content in astrocytes which results in reactive gliosis in the hippocampus and other brain

regions (31, 45, 51, 52, 54). Until recently it was unclear whether the reactive astrogliosis in the epileptic foci was a cause or a consequence of epileptiform spiking activity (15-17, 20, 55, 56). We had demonstrated reactive astrogliosis in the hippocampus in the C57BL/6J mouse kainate model at 3 day post-SE (31). In the present study, the reactive astrogliosis and neurodegeneration persisted for up to 28 days, and reactive microgliosis for up to 14 days after the SE in the hippocampus, the entorhinal cortex, and the amygdala. Continuous video-EEG monitoring after inducing the SE revealed maximum number of spontaneous CS during the first 4 weeks when compared to the rest of the 18 weeks study (8). A recent study from a mouse model has shown that a deletion of *integrin-beta1* causes widespread reactive astrogliosis and SRS during the first six weeks of postnatal life (57). Several other studies also support the view that reactive astrocytes contribute to epileptogenesis and SRS (15, 17, 20, 56). The astrocytes under a physiological condition prevent hyperexcitability of neurons by re-uptake of extracellular glutamate and ions at the synaptic terminal, which is compromised in reactive glial cells (58-62). By 28 day post-SE in the present study, there was a reduction in the reactive
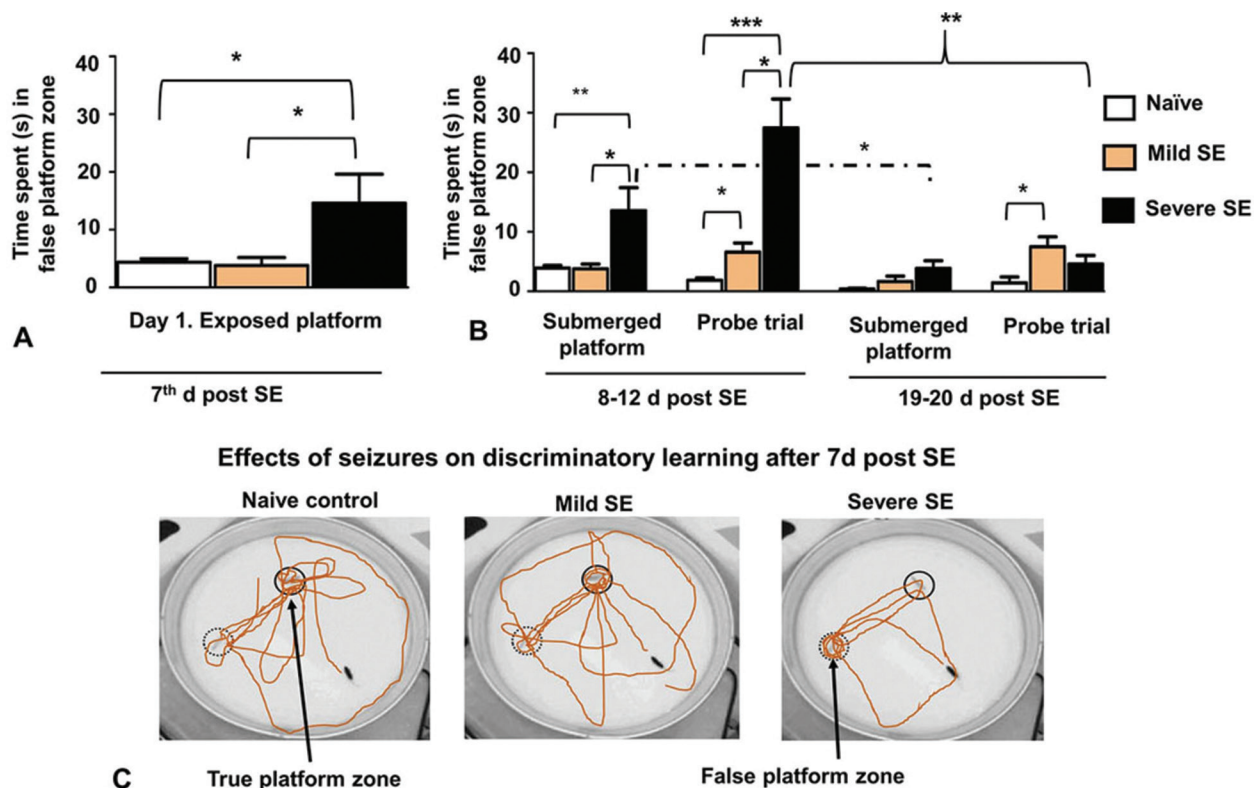
Figure 11. The impact of seizure severity, epileptiform spikes, reactive gliosis, neurodegeneration and neurogenesis on discriminatory learning behavior during the 7-20 days post-SE. The hippocampal dependent spatial learning was tested using the Morris Water Maze. A. The training was started for all three groups at 7th d post-SE to identify the exposed platform (5 trials). There were no differences between the control and the mild SE group in time spent to find the exposed platform. The severe SE group spent significantly more time at the false platform zone (incorrect learning) when compared to the mild SE and the control groups (n=16 for control, and 6 each for the severe and mild group; *p=0.026 for the control and *p=0.029 for the mild group, Mann-Whitney test). B. During the submerged platform trails (5 trials/animal each day for 4 days) from day 8 to 11 post-SE, the severe SE group continued to spend more time to find the submerged platform than the mild and the control groups (p=0.0018, Mann-Whitney test). Later, the single probe trial performed on the 12th day revealed that both the mild SE group spent a significant amount of time at the false zone than the control group (p less than 0.05, Mann-Whitney test). The severe group had further reinforced their incorrect learning behavior by spending more time at the false zone when compared with the control and the mild group (p=0.0018, Mann-Whitney test). On the day 19d, a brief re-training (5 trials) was given to all the three groups to find the submerged platform and a single probe trial was performed on the day 20. At 19d and 20d tests, there was a significant reduction in the time spent in the false platform zone in the severe group when compared to the earlier time points (p=0.002, Mann-Whitney test) suggesting an improvement in their discriminatory learning behavior. There was a small but significant increase in time spent in the false platform between the control and the mild SE mice (p=0.036, Mann-Whitney test) also suggesting a decline in their discriminatory learning behavior. C. The tracks of representative mice from each group travelled during the probe trail is presented.

astrogliosis that also coincided with the reduction in the spontaneous CS suggesting possible role for reactive astrocytes in hyperexcitability of neurons and SRS at earlier time points.

The reactive microglial cells were also increased in the hippocampus during the first 2 week of the SE in this study. At day 3 of post-SE in the C57BL/6J mice we had shown that the stratum pyramidale of the CA regions were invaded by reactive microglial cells with no evidence of neurodegenerative changes (31). At 7 day post-SE in the present study, a similar pattern of the reactive microglial cells invading the stratum pyramidale was evident in the CA3 region of the hippocampus (Figure 6A, iv), and the microglial cells were hypertrophic, which coincided with the neurodegenerative changes observed in the similar area of the hippocampus (Figure 6A, v). It has

been shown that the downstream of SE-induced reactive gliosis increases the production of pro-inflammatory cytokines, chemokines and inducible nitric oxide (NO) synthase (30, 46, 63-65). In an organophosphate model of SE, an increased NO metabolites levels by 4-8 folds and a concomitant decreased ATP levels by 34-60 percent were reported in the hippocampus, and these levels persisted for up to 3 days post-SE (66, 67). These factors seems to exacerbate hyperexcitability of neurons during early epileptogenesis which was evident from the increased spiking activity on the EEG in the present study (Figure 2). Excessive amounts of reactive oxygen and nitrogen species, hyperexcitability of neurons and reactive gliosis are all known to cause neurodegeneration (8, 66-70). In the present study, we have demonstrated increased neurodegeneration in the hippocampus and the hilus of the dentate gyrus, the

entorhinal cortex and the amygdala during the first few weeks of the SE (Figures 6 and 8).

The unique feature of the C57BL/6J mouse kainate model of epilepsy is that the frequency of spontaneous CS decreases after 4 weeks but the electrographic NCS persist beyond this period for up to 18 weeks (8). Other studies have also reported the impact of the severity of SE on hippocampal neurogenesis, aberrant migration of neuroblasts, and SRS in the Swiss mouse kainate, and the rat electroconvulsive and kainate models (4, 71-76). In the present study, both mild and severe SE increased reactive gliosis, neurodegeneration and DCX positive neuroblasts in the subgranular cell layer, the hilus and the dentate granule cell layer at 7 and 14 days post-SE. These changes were also coincided with an increase in the frequency of epileptiform spiking and spontaneous CS during this period (Figure 2). At 28d post-SE, these neurobiological changes were significantly reduced (Figure 10) and also the spontaneous CS (8). The role of enhanced neurogenesis during early post-SE is controversial whether it exacerbate or mitigate spontaneous seizures (14, 36, 47, 77). A recent study demonstrated a direct link between aberrant hippocampal neurogenesis, epilepsy and cognitive decline (78). In the nerve agent (soman) induced SE rat model, diazepam and valproic acid treatment increased neurogenesis and reduced spontaneous seizures (47). In the rat pilocarpine model with severe SE, an increased neurogenesis was reported in the hippocampus at 3 and 7 day post-SE (76), which supports our current findings (Figure 10). Triple immunostaining of brain sections at 7 day post-SE for GFAP, NeuN and DAPI indicated that a subpopulation of SGZ cells were neither GFAP nor NeuN positive (Figure 9A), which were indeed the neuroblasts stained for DCX (Figure 10A). The DCX positive cells were also found in the hilus and dentate granule cell layers. It has been reported that the newborn dentate granule cells synchronize with the host dentate granule cell layer (79, 80). However, aberrant migration of neuroblasts could lead to epileptogenesis (76, 78). Whether the DCX positive cells in the hilus assuming that they originated from the subgranular zone (14, 81, 82), or they migrated from the medial ganglionic eminence (83, 84) needs further investigation.

The neurobiological evidence of hippocampal reactive gliosis and neurodegeneration resulting from the seizures, or vice versa, whether mild or severe, are most likely to have an impact on hippocampus mediated learning and memory tasks. Seizures are known to affect cognitive function (78, 85-87). In the present study, both mild and severe groups showed a significant impairment in learning and memory during the first 1-3 weeks post-SE. This coincided with increased reactive gliosis, neurodegeneration and epileptiform spiking. Epileptiform spiking is known to cause cognitive impairment (88-91). In the present study, although the epileptiform spiking on the EEG persisted for a longer period, the cognitive impairment was more pronounced during the first two weeks of the SE. We did not test the cognitive function beyond 28 days in the present study since the spontaneous seizures were reduced after 4 weeks post-SE (8).

In summary, we were able to detect the neurobiological changes such as gliosis and neurodegeneration in early epileptic phase in C57BL/6J mice that were correlated with the increased spike frequency on the EEG and cognitive dysfunction. A recovery from spontaneous CS, but not from spontaneous electrographic NCS, in this unique regressive mouse model of epilepsy also coincided with a reduction in gliosis, neurodegeneration, decreased spike rate at 28 day post-SE, which was preceded by an increased neurogenesis at 7 and 14 day post-SE. Since, these neurobiological changes occurs in less than four weeks of SE, the C57BL/6J mouse kainate model provides an earliest opportunity to test the effect of intervention drugs while, reducing the cost and duration of experiments when compared to rat models of epilepsy.

6. ACKNOWLEDGEMENTS

7. REFERENCES

1. P. E. Schauwecker: The effects of glycemic control on seizures and seizure-induced excitotoxic cell death. *BMC Neurosci*, 13, 94 (2012)
DOI: 10.1186/1471-2202-13-94

2. P. E. Schauwecker and O. Steward: Genetic determinants of susceptibility to excitotoxic cell death: implications for gene targeting approaches. *Proc Natl Acad Sci* U S A, 94(8), 4103-8 (1997)
DOI: 10.1073/pnas.94.8.4103

3. G. M. McKhann, 2nd, H. J. Wenzel, C. A. Robbins, A. A. Sosunov and P. A. Schwartzkroin: Mouse strain differences in kainic acid sensitivity, seizure behavior, mortality, and hippocampal pathology. *Neuroscience*, 122(2), 551-61 (2003)
DOI: 10.1016/S0306-4522(03)00562-1

4. J. Yang, B. Houk, J. Shah, K. F. Hauser, Y. Luo, G. Smith, E. Schauwecker and G. N. Barnes: Genetic background regulates semaphorin gene expression and epileptogenesis in mouse brain after kainic acid status epilepticus. *Neuroscience*, 131(4), 853-69 (2005)
DOI: 10.1016/j.neuroscience.2004.09.064

5. P. E. Schauwecker: Genetic basis of kainate-induced excitotoxicity in mice: phenotypic modulation of seizure-induced cell death. *Epilepsy Res*, 55(3), 201-10 (2003)
DOI: 10.1016/S0920-1211(03)00115-3

6. S. A. Benkovic, J. P. O'Callaghan and D. B. Miller: Regional neuropathology following kainic acid intoxication in adult and aged C57BL/6J mice. *Brain Res*, 1070(1), 215-31 (2006)
DOI: 10.1016/j.brainres.2005.11.065

7. M. C. McCord, A. Lorenzana, C. S. Bloom, Z. O. Chancer and P. E. Schauwecker: Effect of age on kainate-induced seizure severity and cell death. *Neuroscience*, 154(3), 1143-53 (2008)
DOI: 10.1016/j.neuroscience.2008.03.082

8. S. Puttachary, S. Sharma, K. Tse, E. Beamer, A. Sexton, J. Crutison and T. Thippeswamy: Immediate Epileptogenesis after Kainate-Induced Status Epilepticus in C57BL/6J Mice: Evidence from Long Term Continuous Video-EEG Telemetry. *PLoS One*, 10(7), e0131705 (2015)
DOI: 10.1371/journal.pone.0131705

9. K. Tse, S. Puttachary, E. Beamer, G. J. Sills and T. Thippeswamy: Advantages of Repeated Low Dose against Single High Dose of Kainate in C57BL/6J Mouse Model of Status Epilepticus: Behavioral and Electroencephalographic Studies. *PLoS One*, 9(5), e96622 (2014)
DOI: 10.1371/journal.pone.0096622

10. P. S. Buckmaster and A. L. Jongen-Relo: Highly specific neuron loss preserves lateral inhibitory circuits in the dentate gyrus of kainate-induced epileptic rats. *J Neurosci*, 19(21), 9519-29 (1999)

11. M. S. Rao, B. Hattiangady, D. S. Reddy and A. K. Shetty: Hippocampal neurodegeneration, spontaneous seizures, and mossy fiber sprouting in the F344 rat model of temporal lobe epilepsy. *J Neurosci* Res, 83(6), 1088-105 (2006)

DOI: 10.1002/jnr.20802

12. A. P. Le and W. J. Friedman: Matrix metalloproteinase-7 regulates cleavage of pro-nerve growth factor and is neuroprotective following kainic acid-induced seizures. *J Neurosci*, 32(2), 703-12 (2012)
DOI: 10.1523/JNEUROSCI.4128-11.2012

13. K. M. Chiu, C. C. Wu, M. J. Wang, M. Y. Lee and S. J. Wang: Protective effects of bupivacaine against kainic acid-induced seizure and neuronal cell death in the rat hippocampus. *Biol Pharm Bull*, 38(4), 522-30 (2015)
DOI: 10.1248/bpb.b14-00633

14. J. M. Parent and D. H. Lowenstein: Seizure-induced neurogenesis: are more new neurons good for an adult brain? *Prog Brain Res*, 135, 121-31 (2002)
DOI: 10.1016/S0079-6123(02)35012-X

15. D. K. Binder and C. Steinhauser: Functional changes in astroglial cells in epilepsy. *Glia*, 54(5), 358-68 (2006)
DOI: 10.1002/glia.20394

16. M. L. Olsen and H. Sontheimer: Functional implications for Kir4.1. channels in glial biology: from K^+ buffering to cell differentiation. *J Neurochem*, 107(3), 589-601 (2008)
DOI: 10.1111/j.1471-4159.2008.05615.x

17. J. Wetherington, G. Serrano and R. Dingledine: Astrocytes in the epileptic brain. *Neuron*, 58(2), 168-78 (2008)
DOI: 10.1016/j.neuron.2008.04.002

18. W. Zhang, R. Yamawaki, X. Wen, J. Uhl, J. Diaz, D. A. Prince and P. S. Buckmaster: Surviving hilar somatostatin interneurons enlarge, sprout axons, and form new synapses with granule cells in a mouse model of temporal lobe epilepsy. J *Neurosci*, 29(45), 14247-56 (2009)
DOI: 10.1523/JNEUROSCI.3842-09.2009

19. N. C. de Lanerolle, T. S. Lee and D. D. Spencer: Astrocytes and epilepsy. *Neurotherapeutics*, 7(4), 424-38 (2010)
DOI: 10.1016/j.nurt.2010.08.002

20. G. Seifert, G. Carmignoto and C. Steinhauser: Astrocyte dysfunction in epilepsy. *Brain Res Rev*, 63(1-2), 212-21 (2009)
DOI: 10.1016/j.brainresrev.2009.10.004

21. J. Kessler and H. J. Markowitsch: Different neuropathological effects of intrahippocampal injections of kainic acid and tetanus toxin.

Experientia, 39(8), 922-4 (1983)
DOI: 10.1007/BF01990440

22. W. A. Turski, E. A. Cavalheiro, Z. A. Bortolotto, L. M. Mello, M. Schwarz and L. Turski: Seizures produced by pilocarpine in mice: a behavioral, electroencephalographic and morphological analysis. *Brain Res*, 321(2), 237-53 (1984)
DOI: 10.1016/0006-8993(84)90177-X

23. Y. Ben-Ari and R. Cossart: Kainate, a double agent that generates seizures: two decades of progress. *Trends Neurosci*, 23(11), 580-7 (2000)
DOI: 10.1016/S0166-2236(00)01659-3

24. I. Knuesel, V. Riban, R. A. Zuellig, M. C. Schaub, R. M. Grady, J. R. Sanes and J. M. Fritschy: Increased vulnerability to kainate-induced seizures in utrophin-knockout mice. *Eur J Neurosci,* 15(9), 1474-84 (2002)
DOI: 10.1046/j.1460-9568.2002.01980.x

25. C. Huneau, P. Benquet, G. Dieuset, A. Biraben, B. Martin and F. Wendling: Shape features of epileptic spikes are a marker of epileptogenesis in mice. *Epilepsia,* 54(12), 2219-27 (2013)
DOI: 10.1111/epi.12406

26. R. J. Racine: Modification of seizure activity by electrical stimulation. II. Motor seizure. *Electroencephalogr Clin Neurophysiol,* 32(3), 281-94 (1972)
DOI: 10.1016/0013-4694(72)90177-0

27. R. Morris: Developments of a water-maze procedure for studying spatial learning in the rat. *J Neurosci Methods*, 11(1), 47-60 (1984)
DOI: 10.1016/0165-0270(84)90007-4

28. C. V. Vorhees and M. T. Williams: Morris water maze: procedures for assessing spatial and related forms of learning and memory. *Nat Protoc,* 1(2), 848-58 (2006)
DOI: 10.1038/nprot.2006.116

29. C. A. Schneider, W. S. Rasband and K. W. Eliceiri: NIH Image to ImageJ: 25 years of image analysis. *Nat Methods,* 9(7), 671-5 (2012)
DOI: 10.1038/nmeth.2089

30. A. S. Cosgrave, J. S. McKay, V. Bubb, R. Morris, J. P. Quinn and T. Thippeswamy: Regulation of activity-dependent neuroprotective protein (ADNP) by the NO-cGMP pathway in the hippocampus during kainic acid-induced

seizure. *Neurobiol Dis,* 30(3), 281-92 (2008)
DOI: 10.1016/j.nbd.2008.02.005

31. E. Beamer, J. Otahal, G. J. Sills and T. Thippeswamy: N (w) -propyl-L-arginine (L-NPA) reduces status epilepticus and early epileptogenic events in a mouse model of epilepsy: behavioural, EEG and immunohistochemical analyses. *Eur J Neurosci,* 36(9), 3194-203 (2012)
DOI: 10.1111/j.1460-9568.2012.08234.x

32. A. S. Cosgrave, J. S. McKay, R. Morris, J. P. Quinn and T. Thippeswamy: The effects of nitric oxide inhibition prior to kainic acid treatment on neuro- and gliogenesis in the rat dentate gyrus *in vivo* and *in vitro*. *Histol Histopathol*, 25(7), 841-56 (2010)

33. L. C. Schmued and J. F. Bowyer: Methamphetamine exposure can produce neuronal degeneration in mouse hippocampal remnants. *Brain Res*, 759(1), 135-40 (1997)
DOI: 10.1016/S0006-8993(97)00173-X

34. L. C. Schmued and K. J. Hopkins: Fluoro-Jade B: a high affinity fluorescent marker for the localization of neuronal degeneration. *Brain Res,* 874(2), 123-30 (2000)
DOI: 10.1016/S0006-8993(00)02513-0

35. M. S. Todorovic, M. L. Cowan, C. A. Balint, C. Sun and J. Kapur: Characterization of status epilepticus induced by two organophosphates in rats. *Epilepsy Res,* 101(3), 268-76 (2012)
DOI: 10.1016/j.eplepsyres.2012.04.014

36. A. S. Cosgrave, J. S. McKay and T. Thippeswamy: Differential regulation of vasoactive intestinal peptide (VIP) in the dentate gyrus and hippocampus via the NO-cGMP pathway following kainic acid-induced seizure in the rat. *J Mol Neurosci,* 42(3), 359-69 (2010)
DOI: 10.1007/s12031-010-9353-x

37. M. J. Carson, J. Crane and A. X. Xie: Modeling CNS microglia: the quest to identify predictive models. *Drug Discov Today Dis Models,* 5(1), 19-25 (2008)
DOI: 10.1016/j.ddmod.2008.07.006

38. D. S. Davis and M. J. Carson: An introduction to CNS-Resident Microglia: Definitions, Assays and Functional Roles in Health and Disease. Springer Press, (2013)

39. V. C. Kurschner, R. L. Petruzzi, G. T. Golden, W. H. Berrettini and T. N. Ferraro: Kainate and

AMPA receptor binding in seizure-prone and seizure-resistant inbred mouse strains. *Brain Res,* 780(1), 1-8 (1998)
DOI: 10.1016/S0006-8993(97)01081-0

40. J. P. McLin, L. M. Thompson and O. Steward: Differential susceptibility to striatal neurodegeneration induced by quinolinic acid and kainate in inbred, outbred and hybrid mouse strains. *Eur J Neurosci,* 24(11), 3134-40 (2006)
DOI: 10.1111/j.1460-9568.2006.05198.x

41. P. E. Schauwecker: The relevance of individual genetic background and its role in animal models of epilepsy. *Epilepsy Res,* 97(1-2), 1-11 (2011)
DOI: 10.1016/j.eplepsyres.2011.09.005

42. P. A. Williams, A. M. White, S. Clark, D. J. Ferraro, W. Swiercz, K. J. Staley and F. E. Dudek: Development of spontaneous recurrent seizures after kainate-induced status epilepticus. *J Neurosci,* 29(7), 2103-12 (2009)
DOI: 10.1523/JNEUROSCI.0980-08.2009

43. K. J. Staley, A. White and F. E. Dudek: Interictal spikes: harbingers or causes of epilepsy? *Neurosci Lett,* 497(3), 247-50 (2011)
DOI: 10.1016/j.neulet.2011.03.070

44. D. M. de Groot, E. P. Bierman, P. L. Bruijnzeel, P. Carpentier, B. M. Kulig, G. Lallement, B. P. Melchers, I. H. Philippens and A. H. van Huygevoort: Beneficial effects of TCP on soman intoxication in guinea pigs: seizures, brain damage and learning behaviour. *J Appl Toxicol,* 21 Suppl 1, S57-65 (2001)
DOI: 10.1002/jat.812

45. T. Ravizza, M. Rizzi, C. Perego, C. Richichi, J. Veliskova, S. L. Moshe, M. G. De Simoni and A. Vezzani: Inflammatory response and glia activation in developing rat hippocampus after status epilepticus. *Epilepsia,* 46 Suppl 5, 113-7 (2005)
DOI: 10.1111/j.1528-1167.2005.01006.x

46. A. Vezzani, T. Ravizza, S. Balosso and E. Aronica: Glia as a source of cytokines: implications for neuronal excitability and survival. *Epilepsia,* 49 Suppl 2, 24-32 (2008)
DOI: 10.1111/j.1528-1167.2008.01490.x

47. M. de Araujo Furtado, F. Rossetti, S. Chanda and D. Yourick: Exposure to nerve agents: from status epilepticus to neuroinflammation, brain damage, neurogenesis and epilepsy. *Neurotoxicology,* 33(6), 1476-90 (2012)
DOI: 10.1016/j.neuro.2012.09.001

48. J. Jiang, M. S. Yang, Y. Quan, P. Gueorguieva, T. Ganesh and R. Dingledine: Therapeutic window for cyclooxygenase-2 related anti-inflammatory therapy after status epilepticus. *Neurobiol Dis,* 76, 126-36 (2015)
DOI: 10.1016/j.nbd.2014.12.032

49. G. M. Arisi, M. L. Foresti, K. Katki and L. A. Shapiro: Increased CCL2, CCL3, CCL5, and IL-1beta cytokine concentration in piriform cortex, hippocampus, and neocortex after pilocarpine-induced seizures. *J Neuroinflammation,* 12(1), 129 (2015)
DOI: 10.1186/s12974-015-0347-z

50. P. Carpentier, I. S. Delamanche, M. Le Bert, G. Blanchet and C. Bouchaud: Seizure-related opening of the blood-brain barrier induced by soman: possible correlation with the acute neuropathology observed in poisoned rats. *Neurotoxicology,* 11(3), 493-508 (1990)

51. R. Kovacs, U. Heinemann and C. Steinhauser: Mechanisms underlying blood-brain barrier dysfunction in brain pathology and epileptogenesis: role of astroglia. *Epilepsia,* 53 Suppl 6, 53-9 (2012)
DOI: 10.1111/j.1528-1167.2012.03703.x

52. U. Heinemann, D. Kaufer and A. Friedman: Blood-brain barrier dysfunction, TGFbeta signaling, and astrocyte dysfunction in epilepsy. *Glia,* 60(8), 1251-7 (2012)
DOI: 10.1002/glia.22311

53. H. J. Shin, H. Kim, R. W. Heo, H. J. Kim, W. S. Choi, H. M. Kwon and G. S. Roh: Tonicity-responsive enhancer binding protein haplodeficiency attenuates seizure severity and NF-kappaB-mediated neuroinflammation in kainic acid-induced seizures. *Cell Death Differ,* 21(7), 1095-106 (2014)
DOI: 10.1038/cdd.2014.29

54. F. Frigerio, A. Frasca, I. Weissberg, S. Parrella, A. Friedman, A. Vezzani and F. M. Noe: Long-lasting pro-ictogenic effects induced *in vivo* by rat brain exposure to serum albumin in the absence of concomitant pathology. *Epilepsia,* 53(11), 1887-97 (2012)
DOI: 10.1111/j.1528-1167.2012.03666.x

55. L. A. Shapiro, M. J. Korn, Z. Shan and C. E. Ribak: GFAP-expressing radial glia-like cell bodies are involved in a one-to-one

relationship with doublecortin-immunolabeled newborn neurons in the adult dentate gyrus. *Brain Res,* 1040(1-2), 81-91 (2005)
DOI: 10.1016/j.brainres.2005.01.098

56. M. B. Gibbons, R. M. Smeal, D. K. Takahashi, J. R. Vargas and K. S. Wilcox: Contributions of astrocytes to epileptogenesis following status epilepticus: opportunities for preventive therapy? *Neurochem Int,* 63(7), 660-9 (2012)
DOI: 10.1016/j.neuint.2012.12.008

57. S. Robel, S. C. Buckingham, J. L. Boni, S. L. Campbell, N. C. Danbolt, T. Riedemann, B. Sutor and H. Sontheimer: Reactive astrogliosis causes the development of spontaneous seizures. *J Neurosci,* 35(8), 3330-45 (2015)
DOI: 10.1523/JNEUROSCI.1574-14.2015

58. A. Bordey and H. Sontheimer: Passive glial cells, fact or artifact? J Membr Biol, 166(3), 213-22 (1998)
DOI: 10.1007/s002329900463

59. A. Bordey, S. A. Lyons, J. J. Hablitz and H. Sontheimer: Electrophysiological characteristics of reactive astrocytes in experimental cortical dysplasia. *J Neurophysiol*, 85(4), 1719-31 (2001)

60. A. Volterra and J. Meldolesi: Astrocytes, from brain glue to communication elements: the revolution continues. *Nat Rev Neurosci,* 6(8), 626-40 (2005)
DOI: 10.1038/nrn1722

61. C. Steinhauser and G. Seifert: Astrocyte dysfunction in epilepsy. *Brain Res Rev,* 63 (1-2), 212-21 (2010)
DOI: 10.1016/j.brainresrev.2009.10.004

62. T. Eid, N. Tu, T. S. Lee and J. C. Lai: Regulation of astrocyte glutamine synthetase in epilepsy. *Neurochem Int,* 63(7), 670-81 (2013)
DOI: 10.1016/j.neuint.2013.06.008

63. F. J. Perez-Asensio, O. Hurtado, M. C. Burguete, M. A. Moro, J. B. Salom, I. Lizasoain, G. Torregrosa, J. C. Leza, E. Alborch, J. Castillo, R. G. Knowles and P. Lorenzo: Inhibition of iNOS activity by 1400W decreases glutamate release and ameliorates stroke outcome after experimental ischemia. *Neurobiol Dis,* 18(2), 375-84 (2005)
DOI: 10.1016/j.nbd.2004.10.018

64. M. Jafarian-Tehrani, G. Louin, N. C. Royo, V. C. Besson, G. A. Bohme, M. Plotkine and C. Marchand-Verrecchia: 1400W, a potent selective inducible NOS inhibitor, improves histopathological outcome following traumatic brain injury in rats. *Nitric Oxide,* 12(2), 61-9 (2005)
DOI: 10.1016/j.niox.2004.12.001

65. E. Aronica, U. S. Sandau, A. Iyer and D. Boison: Glial adenosine kinase--a neuropathological marker of the epileptic brain. *Neurochem Int,* 63(7), 688-95 (2013)
DOI: 10.1016/j.neuint.2013.01.028

66. R. C. Gupta, D. Milatovic and W. D. Dettbarn: Depletion of energy metabolites following acetylcholinesterase inhibitor-induced status epilepticus: protection by antioxidants. *Neurotoxicology,* 22(2), 271-82 (2001)
DOI: 10.1016/S0161-813X(01)00013-4

67. R. C. Gupta, D. Milatovic and W. D. Dettbarn: Nitric oxide modulates high-energy phosphates in brain regions of rats intoxicated with diisopropylphosphorofluoridate or carbofuran: prevention by N-tert-butyl-alpha-phenylnitrone or vitamin E. *Arch Toxicol,* 75(6), 346-56 (2001)
DOI: 10.1007/s002040100249

68. H. Ischiropoulos: Biological tyrosine nitration: a pathophysiological function of nitric oxide and reactive oxygen species. *Arch Biochem Biophys*, 356(1), 1-11 (1998)
DOI: 10.1006/abbi.1998.0755

69. M. J. Bianchetta, T. T. Lam, S. N. Jones and M. A. Morabito: Cyclin-dependent kinase 5 regulates PSD-95 ubiquitination in neurons. *J Neurosci,* 31(33), 12029-35 (2011)
DOI: 10.1523/JNEUROSCI.2388-11.2011

70. C. Liu, Y. Li, P. J. Lein and B. D. Ford: Spatiotemporal patterns of GFAP upregulation in rat brain following acute intoxication with diisopropylfluorophosphate (DFP). *Curr Neurobiol,* 3(2), 90-97 (2012)

71. J. M. Parent, R. C. Elliott, S. J. Pleasure, N. M. Barbaro and D. H. Lowenstein: Aberrant seizure-induced neurogenesis in experimental temporal lobe epilepsy. *Ann Neurol,* 59(1), 81-91 (2006)
DOI: 10.1002/ana.20699

72. J. M. Parent, T. W. Yu, R. T. Leibowitz, D. H. Geschwind, R. S. Sloviter and D. H. Lowenstein: Dentate granule cell neurogenesis is increased by seizures and contributes to aberrant network reorganization

in the adult rat hippocampus. *J Neurosci,* 17(10), 3727-38 (1997)

73. P. Mohapel, C. T. Ekdahl and O. Lindvall: Status epilepticus severity influences the long-term outcome of neurogenesis in the adult dentate gyrus. *Neurobiol Dis,* 15(2), 196-205 (2004)
DOI: 10.1016/j.nbd.2003.11.010

74. F. Yang, J. C. Wang, J. L. Han, G. Zhao and W. Jiang: Different effects of mild and severe seizures on hippocampal neurogenesis in adult rats. Hippocampus, 18(5), 460-8 (2008)
DOI: 10.1002/hipo.20409

75. V. Bouilleret, V. Ridoux, A. Depaulis, C. Marescaux, A. Nehlig and G. Le Gal La Salle: Recurrent seizures and hippocampal sclerosis following intrahippocampal kainate injection in adult mice: electroencephalography, histopathology and synaptic reorganization similar to mesial temporal lobe epilepsy. *Neuroscience,* 89(3), 717-29 (1999)
DOI: 10.1016/S0306-4522(98)00401-1

76. Y. W. Hung, D. I. Yang, P. Y. Huang, T. S. Lee, T. B. Kuo, C. H. Yiu, Y. H. Shih and Y. Y. Lin: The duration of sustained convulsive seizures determines the pattern of hippocampal neurogenesis and the development of spontaneous epilepsy in rats. *Epilepsy Res,* 98(2-3), 206-15 (2012)
DOI: 10.1016/j.eplepsyres.2011.09.015

77. P. Jiruska, A. B. Shtaya, D. M. Bodansky, W. C. Chang, W. P. Gray and J. G. Jefferys: Dentate gyrus progenitor cell proliferation after the onset of spontaneous seizures in the tetanus toxin model of temporal lobe epilepsy. *Neurobiol Dis*, 54, 492-8 (2013)
DOI: 10.1016/j.nbd.2013.02.001

78. K. O. Cho, Z. R. Lybrand, N. Ito, R. Brulet, F. Tafacory, L. Zhang, L. Good, K. Ure, S. G. Kernie, S. G. Birnbaum, H. E. Scharfman, A. J. Eisch and J. Hsieh: Aberrant hippocampal neurogenesis contributes to epilepsy and associated cognitive decline. *Nat Commun*, 6, 6606 (2015)
DOI: 10.1038/ncomms7606

79. H. E. Scharfman, J. H. Goodman and A. L. Sollas: Granule-like neurons at the hilar/ CA3 border after status epilepticus and their synchrony with area CA3 pyramidal cells: functional implications of seizure-induced neurogenesis. *J Neurosci*, 20(16),

6144-58 (2000)

80. B. L. Murphy, R. Y. Pun, H. Yin, C. R. Faulkner, A. W. Loepke and S. C. Danzer: Heterogeneous integration of adult-generated granule cells into the epileptic brain. *J Neurosci*, 31(1), 105-17 (2011)
DOI: 10.1523/JNEUROSCI.2728-10.2011

81. H. E. Scharfman, A. E. Sollas, R. E. Berger, J. H. Goodman and J. P. Pierce: Perforant path activation of ectopic granule cells that are born after pilocarpine-induced seizures. *Neuroscience*, 121(4), 1017-29 (2003)
DOI: 10.1016/S0306-4522(03)00481-0

82. S. C. Danzer, X. He, A. W. Loepke and J. O. McNamara: Structural plasticity of dentate granule cell mossy fibers during the development of limbic epilepsy. *Hippocampus*, 20(1), 113-24 (2009)
DOI: 10.1002/hipo.20589

83. L. Danglot, A. Triller and S. Marty: The development of hippocampal interneurons in rodents. *Hippocampus*, 16(12), 1032-60 (2006)
DOI: 10.1002/hipo.20225

84. K. W. Henderson, J. Gupta, S. Tagliatela, E. Litvina, X. Zheng, M. A. Van Zandt, N. Woods, E. Grund, D. Lin, S. Royston, Y. Yanagawa, G. B. Aaron and J. R. Naegele: Long-term seizure suppression and optogenetic analyses of synaptic connectivity in epileptic mice with hippocampal grafts of GABAergic interneurons. *J Neurosci*, 34(40), 13492-504 (2014)
DOI: 0.1523/JNEUROSCI.0005-14.2014

85. J. N. Lugo, J. W. Swann and A. E. Anderson: Early-life seizures result in deficits in social behavior and learning. *Exp Neurol*, 256, 74-80 (2014)
DOI: 10.1016/j.expneurol.2014.03.014

86. J. A. Witt and C. Helmstaedter: Cognition in the early stages of adult epilepsy. *Seizure*, 26, 65-8 (2015)
DOI: 10.1016/j.seizure.2015.01.018

87. A. P. Jellett, K. Jenks, M. Lucas and R. C. Scott: Standard dose valproic acid does not cause additional cognitive impact in a rodent model of intractable epilepsy. *Epilepsy Res*, 110, 88-94 (2015)
DOI: 10.1016/j.eplepsyres.2014.11.005

88. A. R. Brooks-Kayal, K. G. Bath, A. T. Berg, A.

S. Galanopoulou, G. L. Holmes, F. E. Jensen, A. M. Kanner, T. J. O'Brien, V. H. Whittemore, M. R. Winawer, M. Patel and H. E. Scharfman: Issues related to symptomatic and disease-modifying treatments affecting cognitive and neuropsychiatric comorbidities of epilepsy. *Epilepsia*, 54 Suppl 4, 44-60 (2013)
DOI: 10.1111/epi.12298

89. J. K. Kleen, R. C. Scott, G. L. Holmes, D. W. Roberts, M. M. Rundle, M. Testorf, P. P. Lenck-Santini and B. C. Jobst: Hippocampal interictal epileptiform activity disrupts cognition in humans. *Neurology*, 81(1), 18-24 (2013)
DOI: 10.1212/WNL.0b013e318297ee50

90. G. L. Holmes: EEG abnormalities as a biomarker for cognitive comorbidities in pharmacoresistant epilepsy. *Epilepsia*, 54 Suppl 2, 60-2 (2013)
DOI: 10.1111/epi.12186

91. G. L. Holmes: Cognitive impairment in epilepsy: the role of network abnormalities. *Epileptic Disord*, 17(2), 101-16 (2015)

Send correspondence to: Thimmasettappa Thippeswamy, Department of Biomedical Sciences, College of Veterinary Medicine, Iowa State University, Ames IA 50011-1250, USA, Tel: 515-294-2571, Fax: 515-294-2315 E-mail: tswamy@iastate.edu